Ecological Modelling 409 (2019) 108765

Contents lists available at ScienceDirect

Ecological Modelling

journal homepage: www.elsevier.com/locate/ecolmodel

Importance of tree- and species-level interactions with wildfire, climate, and soils in interior Alaska: Implications for forest change under a warming climate

Adrianna C. Foster[a,b,*], Amanda H. Armstrong[b,c], Jacquelyn K. Shuman[d], Herman H. Shugart[c], Brendan M. Rogers[e], Michelle C. Mack[f], Scott J. Goetz[a], K. Jon Ranson[b]

[a] Northern Arizona University, School of Informatics, Computing, and Cyber Systems, 1295 S. Knoles Dr., Flagstaff, AZ 86011, USA
[b] NASA Goddard Space Flight Center, Code 618, 8800 Greenbelt Rd, Greenbelt, MD 20771, USA
[c] University of Virginia, 376 Clark Hall, 291 McCormick Rd, Charlottesville, VA 22904, USA
[d] National Center for Atmospheric Research, 1850 Table Mesa Drive, Boulder, CO 80305, USA
[e] Woods Hole Research Center, 149 Woods Hole Rd, Falmouth, MA 02540, USA
[f] Northern Arizona University, Center for Ecosystem Science and Society and Department of Biological Sciences, 600 S Knoles Drive, Flagstaff, AZ 86011, USA

ARTICLE INFO

Keywords:
Forest modeling
UVAFME
Boreal forest
Individual-based model
Disturbances
Climate change

ABSTRACT

The boreal zone of Alaska is dominated by interactions between disturbances, vegetation, and soils. These interactions are likely to change in the future through increasing permafrost thaw, more frequent and intense wildfires, and vegetation change from drought and competition. We utilize an individual tree-based vegetation model, the University of Virginia Forest Model Enhanced (UVAFME), to estimate current and future forest conditions across sites within interior Alaska. We updated UVAFME for application within interior Alaska, including improved simulation of permafrost dynamics, litter decay, nutrient dynamics, fire mortality, and post-fire regrowth. Following these updates, UVAFME output on species-specific biomass and stem density was comparable to inventory measurements at various forest types within interior Alaska. We then simulated forest response to climate change at specific inventory locations and across the Tanana Valley River Basin on a $2 \times 2\,km^2$ grid. We derived projected temperature and precipitation from a five-model average taken from the CMIP5 archive under the RCP 4.5 and 8.5 scenarios. Results suggest that climate change and the concomitant impacts on wildfire and permafrost dynamics will result in overall decreases in biomass (particularly for spruce (*Picea* spp.)) within the interior Tanana Valley, despite increases in quaking aspen (*Populus tremuloides*) biomass, and a resulting shift towards higher deciduous fraction. Simulation results also predict increases in biomass at cold, wet locations and at high elevations, and decreases in biomass in dry locations, under both moderate (RCP 4.5) and extreme (RCP 8.5) climate change scenarios. These simulations demonstrate that a highly detailed, species interactive model can be used across a large region within Alaska to investigate interactions between vegetation, climate, wildfire, and permafrost. The vegetation changes predicted here have the capacity to feed back to broader scale climate-forest interactions in the North American boreal forest, a region which contributes significantly to the global carbon and energy budgets.

1. Introduction

High-latitude ecosystems account for about 40% of global terrestrial carbon (C), which is comparable to the global atmospheric C pool (Bradshaw and Warkentin, 2015). The fate of these ecosystems is therefore significant for management and monitoring of C stocks and for understanding climate change trajectories. Surface temperatures in Alaska have increased by roughly 2 °C in the last 60 years, more than twice the rate of warming at lower latitudes (Chapin et al., 2014; Melillo et al., 2014; Overland et al., 2016). Temperatures in Alaska are projected to increase further, by as much as 2–6 °C in the next 50 years (Leonawicz et al., 2015a). This change is dependent, however, on local-

* Corresponding author.
E-mail addresses: Adrianna.Foster@nau.edu (A.C. Foster), amanda.h.armstrong@nasa.gov (A.H. Armstrong), jkshuman@ucar.edu (J.K. Shuman), hhs@virginia.edu (H.H. Shugart), brogers@whrc.org (B.M. Rogers), Michelle.Mack@nau.edu (M.C. Mack), Scott.Goetz@nau.edu (S.J. Goetz), kenneth.j.ranson@nasa.gov (K.J. Ranson).

https://doi.org/10.1016/j.ecolmodel.2019.108765
Received 30 March 2019; Received in revised form 23 July 2019; Accepted 24 July 2019

scale biophysical interactions and global-scale biogeochemical interactions between vegetation, disturbances, and climate (Fettig et al., 2013; Euskirchen et al., 2016), providing an imperative to better understand vegetation-climate feedback dynamics.

Alaska's boreal forest stores large amounts of C, particularly in the soil organic layer, and may be especially vulnerable to climate change-related disturbances (Kasischke et al., 2010; Grosse et al., 2011; Pastick et al., 2017). Wildfires are a dominant and integral component of the Alaskan boreal zone affecting soil C and the species composition, forest age-structure, and successional state of vegetation (Viereck et al., 1986). Climate change within Alaska is likely to generate increased drought and longer fire seasons (Jolly et al., 2015), as well as increases in the severity and frequency of fires (Macias Fauria and Johnson, 2006; Kasischke et al., 2010; Genet et al., 2013). Vegetation composition, structure, and biomass within boreal Alaska is also highly dependent on soil characteristics such as organic layer depth, active layer thickness, and plant-available nutrients (Van Cleve and Viereck, 1981; Shugart et al., 1992; Johnstone et al., 2010a). Reciprocally, vegetation characteristics influence fire frequency and severity through differences in fuel amount and flammability, as well as soil characteristics through species-specific effects on litter quality and decomposition rate (Chapin et al., 2006b; Johnstone et al., 2010a). Combined with uncertainty in the direct impacts of climate change on boreal vegetation (Barber et al., 2000; Andreu-Hayles et al., 2011), these interactions between vegetation, fire, and soils complicate modeling predictions of both current and future vegetation composition and biomass. In fact, a comparison of 40 terrestrial biosphere models found high uncertainty and variability in both the magnitude and sign of the annual C flux over Alaska, with some showing the region as a strong sink and others a strong source for C (Fisher et al., 2014). This uncertainty may in part be due to a lack of treatment of individual trees and individual species within these models, both of which can be important when considering the interactions between climate, fire, vegetation, and soils (Kasischke et al., 2000; Johnstone et al., 2010a; Rogers et al., 2015; Alexander and Mack, 2015). A follow on study by Fisher et al. (2018) cited plant biomass, NPP, GPP, and PFTs as major "missing pieces" to the modeling puzzle in the Artic-Boreal region. Competition between individual trees has also been identified as crucial for understanding vegetation response to climate (Purves and Pacala, 2008). As climate and disturbance regimes continue to change, these interactive drivers may also result in new species mixtures for boreal Alaska that require, in turn, high-resolution species-level modeling.

Ecosystem modeling has been used across Alaska to investigate the response of vegetation to climate and fire using models such as ALFRESCO, TEM, and *ecosys* (Rupp et al., 2007; Euskirchen et al., 2009; Genet et al., 2013; Mekonnen et al., 2019). These models represent vegetation as broad vegetation types and may not fully capture the species- and tree-level interactions between vegetation, soil, and disturbances, or the resulting competitive dynamics at the inherent scale at which they operate (i.e. individual trees). Individual-based forest gap models (IBGMs), which simulate the establishment, growth, and mortality of individual trees (Shugart, 1984; Shugart et al., 2018), can aid in predicting these future interactions through explicit simulation of individual tree response to environmental change, competition with other trees, as well as disturbances. Such tree-level simulation allows for the incorporation of important species- and tree size-specific interactions with organic layer depth, nutrient availability and litter characteristics, permafrost depth, shading from other trees, fire mortality, and seedbank/seedling response to fires.

Forest gap models include both deterministic processes, such as species-specific optimal diameter increment growth over time and individual tree growth response to environmental conditions, as well as stochastic processes such as stress-related mortality and disturbances. Whereas plot-level output represents one potential outcome arising from the incorporation of these processes and interactions, the average of several hundred of such plots represents average expected characteristics of a particular forested landscape of indeterminate size, similar to a random sampling of forest inventory plots. Here we define 'forest landscape' as a dynamic mosaic of forest gaps, each in its own successional stage at any given simulation year (Shugart and Seagle, 1985), which is appropriate for use in the Alaskan boreal zone, where disturbances result in a mosaic of different vegetation structures and composition across the region (Payette, 1992).

Through the aggregation of several hundred plots, gap models simulate emergent properties of forest landscapes over time such as forest succession, cyclical dynamics, and forest response to shifting climate and disturbance regimes (Shugart and Woodward, 2011; Foster et al., 2015; Shuman et al., 2015; Shugart et al., 2018). When applied at sites spanning large regions or continents, they can provide regional estimates of forest characteristics (Shuman et al., 2015; 2017). Therefore, gap models can be used to predict changes in vegetation composition and structure across a wide range of temporal and spatial scales, lending themselves to predicting such potential changes within the Alaskan boreal zone.

The University of Virginia Forest Model Enhanced (UVAFME) is an individual tree-based gap model, and is an update and extension of the gap model FAREAST (Yan and Shugart, 2005). UVAFME has been successfully applied in the North American Rocky Mountains (Foster et al., 2015, 2017), the eastern US (Wang et al., 2017), as well as boreal Russia (Shuman et al., 2015, 2017). Model output has been validated against inventory data and maps of species composition and vegetation type across all of boreal Russia (Shuman et al., 2014, 2015). Despite its success in simulating boreal Russian forests and the relative bioclimatic similarity between boreal Russia and Alaska, initial testing and parameter calibration of UVAFME in Alaska showed that it did not accurately predict species-specific biomass or successional dynamics within the study region. In particular, the model was unable to adequately distinguish between higher biomass white spruce (*Picea glauca)*-dominated sites and lower biomass black spruce (*Picea mariana*)-dominated sites, but rather predicted a mixture of the two spruce species at inventory sites where one was dominant (Fig. A1; A2 in the Appendix). Within boreal Alaska, the relative dominance of black and white spruce leads to differing and often self-perpetuating site and soil conditions (Johnstone et al., 2010a). Black spruce trees are able to grow and reproduce on thick, moist, cold soils (Burns and Honkala, 1990; Viereck and Little, 2007), and the recalcitrant nature of black spruce litter and resultant buildup of the organic layer leads to the subsistence of wet soils, a shallow permafrost layer, and black spruce dominance (Chapin et al., 2006b, Johnstone et al. 2010a). In contrast, white spruce and mixed deciduous sites typically occur on drier, warmer sites without permafrost (Chapin et al., 2006b). Deciduous litter decays more quickly (Flanagan and Van Cleve, 1983; Vance and Chapin, 2001), leading to a thinner organic layer and thus the persistence of a deep active layer. These soil-vegetation dynamics additionally impact the fire regime to create lasting legacies of site conditions.

UVAFME did not previously simulate permafrost depth and freeze/thaw dynamics, dynamic decomposition of different litter classes (e.g. leaves, boles, branches, etc.), or interactions between litter content and moisture and fire dynamics. Because the interactions of disturbances, moisture, permafrost, and nutrients are essential to the heterogeneity of species composition and biomass on the landscape (Van Cleve and Viereck, 1981; Chapin et al., 2006b; Johnstone et al., 2010b), the lack of such relationships likely contributed to the initial inaccuracies in predicting biomass and vegetation type within Alaska. Thus, simulation of these interactions is needed in order to predict current forest characteristics as well as forest response to climate change. We have updated UVAFME to include these crucial relationships and interactions, including simulation of daily permafrost depth and interactions with soil moisture and decomposition, genus- and litter class-specific decomposition in response to site and soil conditions, as well as impacts and interactions of these drivers with individual tree growth, mortality, and regeneration. We additionally updated the existing fire submodel

within UVAFME to incorporate the effects of moss and litter characteristics on fire severity and individual tree fire mortality. The performance of UVAFME following these model updates was tested against data from several locations across boreal Alaska. The updated model was then used to simulate current and potential future forested conditions across the entire Tanana River Basin, at a $2 \times 2\,km^2$ grid resolution. These results highlight the significance of the tree and species-scale interactions among important environmental drivers in the Alaskan boreal forest, and predict the potential future dynamics of this ecosystem.

2. Methods

2.1. Model description

UVAFME simulates the growth, mortality, and regeneration of individual trees on independent $500\,m^2$ plots (roughly $22 \times 22\,m$) of a forested landscape (Yan and Shugart, 2005; Shuman et al., 2015; Foster et al., 2017) (Fig. A3 in the Appendix). While each plot has an area associated with it, the plots are not spatially distributed and they do not interact with one another. Individual tree growth is simulated through annual optimal diameter increment growth, calculated using allometric equations with species-specific growth parameters (Table A1). This optimal growth is then decreased according to the current site and climate conditions as well as species-specific environmental and resource tolerances (i.e. moisture, temperature, nutrient, shade, and now permafrost tolerance). Trees may die from prolonged low diameter growth or by disturbances. Trees regenerate via species-specific seed- and seedling banks, which are modified annually based on current site conditions and species-specific tolerances. Daily weather (i.e. mean temperature (°C), cloud cover (%), and precipitation (cm)) is generated via input distributions of monthly minimum and maximum temperatures, mean cloud cover, and mean monthly precipitation. A full description UVAFME and all of its equations can be found in Foster et al. (2017) and on the UVAFME website (https://uvafme.github.io/).

2.2. Model updates

UVAFME was updated to improve simulation of forest and ecosystem dynamics within the North American boreal region, including updates to the model's climate (Section 2.2.1), soil moisture (Section 2.2.3), decomposition (Section 2.2.4) and fire (Section 2.2.6) subroutines, as well as the development of new permafrost (Section 2.2.2) and moss (Section 2.2.5) subroutines.

2.2.1. Climate

UVAFME's solar radiation subroutine was initially modified to account for the heightened effects of sun angle, slope, and aspect at high latitudes (Rosenberg et al., 1983). Top-of-atmosphere radiation is attenuated through the atmosphere and clouds to derive horizontal surface radiation. Tilt factors based on site topography are then used to calculate the actual solar radiation received at the surface (Liu and Jordan, 1962). Previously, UVAFME used extraterrestrial radiation to calculate potential evapotranspiration (PET) using Hargreaves evaporation formula (Hargreaves and Samni, 1982; Foster et al., 2017). However, this formula does not account for cloud cover nor does it incorporate the effects of topography on PET (Rosenberg et al., 1983), which is an especially important factor at high latitudes and in areas of complex terrain, such as interior Alaska. The formulation for PET was updated for UVAFME to use a modified Priestley-Taylor equation (Jensen and Haise, 1963), as in Bonan (1989), which uses surface solar radiation rather than extraterrestrial radiation. Because surface solar radiation depends on elevation, slope, and aspect (Liu and Jordan, 1962), this change additionally allows for topographic effects on PET and thus soil moisture and permafrost dynamics (see Sections 1 and 2 in Supplementary Material II for full description of code updates and equations).

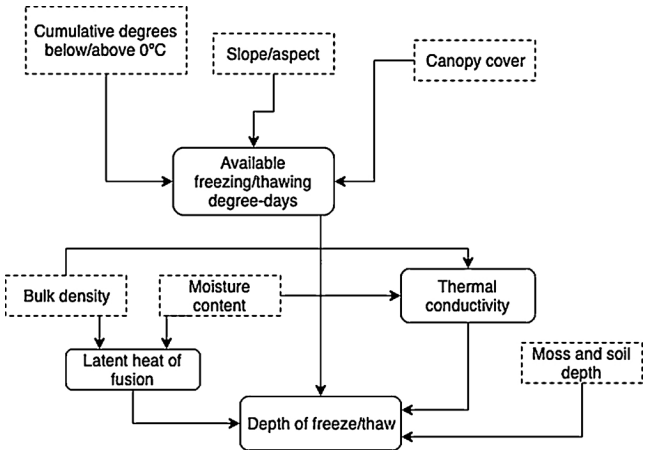

Fig. 1. Conceptual diagram of the permafrost submodel in UVAFME. Dashed boxes indicate inputs into the model, either from other submodels or as input parameters.

2.2.2. Permafrost dynamics

Soil conditions (e.g. moisture, N content, etc.), which previously in UVAFME were assumed to be equal across all simulated plots at a site, were made specific to individual plots in order to incorporate the desired interactions between vegetation, soils, and wildfire. According to this implementation, each plot within a site starts with the same initial soil conditions, but these values may change from plot to plot as the simulation progresses, via differences in vegetation or disturbance occurrences. This plot-level soil interaction allows the model to more directly capture heterogeneity at the landscape-level (i.e. the average of several hundred plots).

We updated UVAFME to include active layer depth and its effect on soil moisture and individual tree growth. Soil dynamics are modeled as a two-layer system consisting of a moss-organic layer (i.e. moss, decaying litter, and soil organic matter representing fibric, mesic, and humic contents) and a mineral (A) layer. For each day in a simulation year, the depths of freezing and thawing are calculated using the Stefan equation (Jumikis, 1966), which is based on soil moisture, depth, and bulk density (Lunardini, 1981; Bonan, 1989) (Fig. 1; Eq. 1).

$$DD_{req} = Q_l d_s / 24 \left(r_{above} + \frac{r_s}{2} \right) \quad (1)$$

where DD_{req} is the required number of freezing/thawing degree-days (i.e. cumulative degrees below/above 0 °C) to completely freeze/thaw a layer of depth d_s (m), Q_l is the latent heat of fusion of the soil layer (kcal m^{-3}), and r_s

and r_{above} are the thermal resistances of the current and above soil/moss layers, respectively (m^2 °C hr $kcal^{-1}$). The latent heat of fusion is calculated based on soil water content and bulk density, and thermal resistance is calculated based on soil depth and soil thermal conductivity, which in turn is also based on soil moisture (Fig. 1). The required degree-days are then compared to simulated freezing/thawing degree-days, modified based on site-level topographic characteristics and plot-level forest canopy cover, to calculate the actual depths of freezing (DD_{f_a}) and thawing (DD_{t_a}) in the soil layer (Eqs. 2,3):

$$DD_{f_a} = DD_f c_f (2 - c_s) \quad (2)$$

$$DD_{t_a} = DD_t c_t c_s \quad (3)$$

where DD_f and DD_t are cumulative freezing/thawing degree-days, and c_f, c_t, and c_s are correction factors based on forest canopy cover and topographic characteristics, with higher available freezing degree-days under dense canopies and north-facing slopes, and higher available

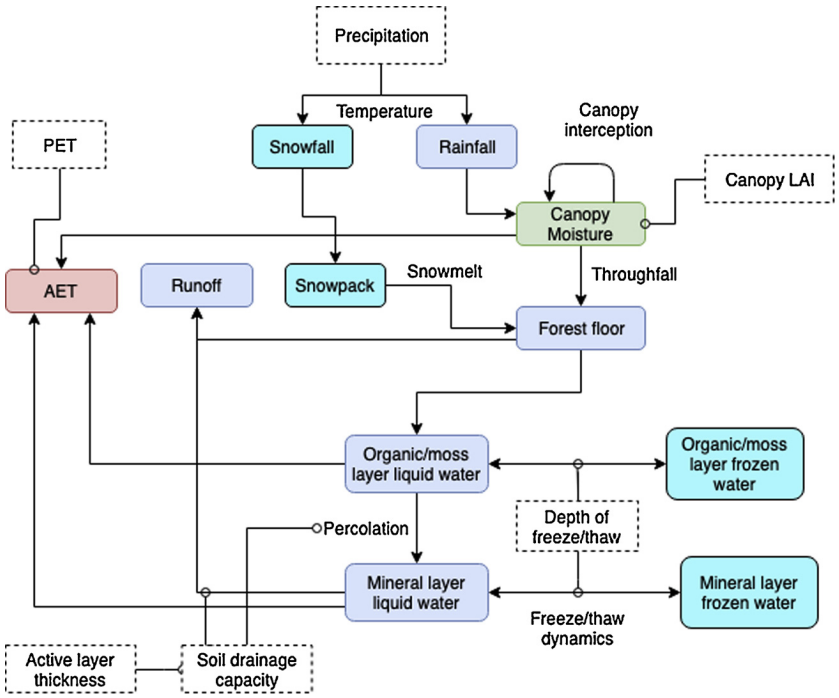

Fig. 2. Conceptual diagram of the updated soil moisture submodel in UVAFME. Dashed boxes indicate inputs into the model, either from other submodels or as input parameters. Blue boxes indicate liquid water pools, cyan represent frozen water pools, green represent canopy moisture, and red represent evaporation.

thawing degree-days under sparse canopies on south-facing slopes (Supplementary Material II).

The associated freezing and thawing depths are used to derive the annual maximum depth of thaw (i.e. active layer thickness). Active layer thickness (alt, m) is then used to modify individual tree growth by decreasing annual diameter increment growth at varying levels depending on species-specific permafrost tolerance (Bonan, 1989) (Eq. 64 in Supplementary Material II).

2.2.3. Soil moisture dynamics

As in Bonan (1989), active layer depth impacts soil drainage capacity, and daily depths of freeze and thaw are used to calculate daily amounts of frozen and liquid water in the organic and mineral layers, thus impacting plant-available water throughout the year as well as across years via changes in active layer thickness (Fig. 2). As with previous versions of UVAFME, precipitation inputs (either liquid rainfall or snow) are partitioned into canopy interception, slope runoff (R_s, m), and throughfall (t_{fall}, m). Daily snowpack accumulation and melt (s_{melt}, m) are also calculated based on temperature. Potential water loss via evaporative demand (negative) or gain via water inputs (positive) is calculated as: $pw = t_{fall} + s_{melt} - R_s - PET$. For each soil layer, the amount of water released in soil thawing (w_t, m) and water frozen (w_f, m) are calculated as (Eqs. 4,5):

$$w_t = z_{drain}(d_{thaw} - d'_{thaw}) \tag{4}$$

$$w_f = \frac{w_l}{d_{thaw}}(d_{freeze} - d'_{freeze}) \tag{5}$$

where w_l is the amount of liquid water in the soil layer (m), d_{thaw} and d'_{thaw} are the current and previous days' depth of thaw (m), d_{freeze} and d'_{freeze} are the current and previous days' depth of freeze (m), and z_{drain} is a drainage parameter based on the seasonal active layer thickness (alt, m), and the soil layer's field capacity (m_{fc}, volumetric) and saturation capacity (m_{sat}, volumetric) (Eq. 6):

$$z_{drain} = \min\left(\max\left(\frac{m_{sat}(1 - alt) + m_{fc}(alt - 0.32)}{1 - 0.32}, m_{fc}\right), m_{sat}\right) \tag{6}$$

The daily depth of thaw is also used to modify each layer's saturation and field capacities and wilting point (Eqs. 21–23 in Supplementary Material II). These values are used to calculate the amount of excess water in each soil layer after accounting for precipitation/snowmelt inputs and soil thawing. Excess water is removed according to a modified equation from Botkin (1993), whereby the amount of soil runoff/percolation increases as the rainfall/water input increases or as the soil layer becomes more saturated (Eq. 24 in Supplementary Material II). Excess water from the moss-organic layer is transferred to the mineral layer, and excess water from the mineral layer is subtracted as runoff.

As in previous versions of UVAFME, if there is a negative water balance (i.e. $pw < 0.0$) from either high PET or low water inputs, water is evaporated from the canopy and soil layers until the evaporative demand is satisfied or no more water can be extracted. Evapotranspiration is dependent on the relative root distribution within each layer (Eqs. 28–31 in Supplementary Material II). Daily soil water contents are used to calculate daily indices of soil dryness and saturation which are aggregated to create annual drought and saturation indices ($\frac{w_l}{m_{fc}}$; $\frac{w_l}{m_{pwp}}$), used throughout the rest of the simulation in the decomposition, moss and tree growth, and fire submodels. See Section 3 in Supplementary Material II for a full description of the soil moisture dynamics updates.

2.2.4. Soil decomposition

In order to simulate the interactions between vegetation composition, decomposition rate, and soil characteristics, the existing soil nutrient dynamics submodel was updated based on equations from Bonan (1990) and Pastor and Post (1985) (Fig. 3). Previously in the model, no distinction was made between different litter types (i.e. branches vs. leaves, etc.) and species. With the updates made in this version, any litter from branch thinning, leaf-off, or tree mortality is added to a litter array, depending on its type (i.e. leaf, twig, small & large boles, root, and moss) and/or genus (for leaf litter). Each year, new litter from each of the types is placed into separate 'cohorts' (defined as decaying organic material ranging from initial loose litter to mostly decomposed, mesic material) that decay until they reach a critical weight, at which

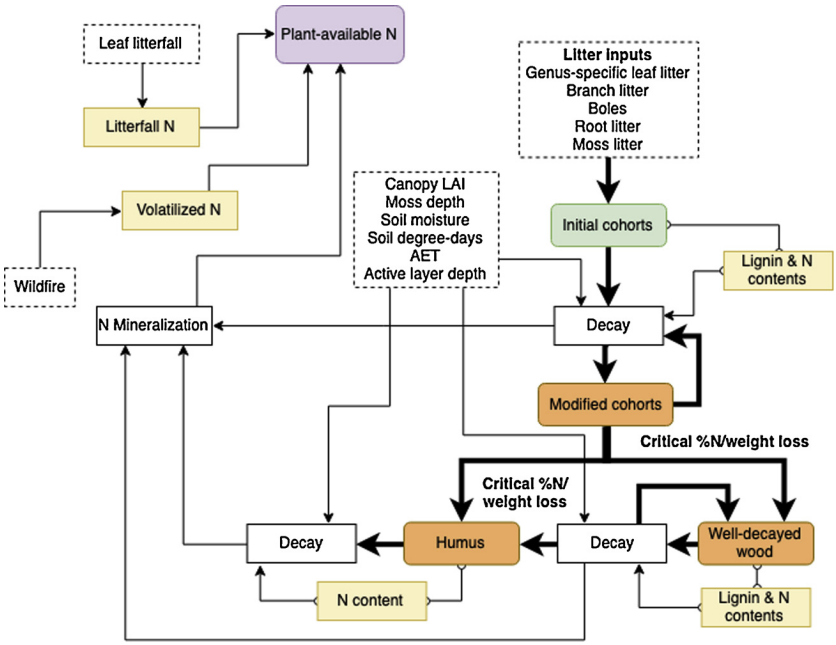

Fig. 3. Conceptual diagram of the updated soil decomposition submodel in UVAFME. Dashed boxes indicate inputs into the model, either from other submodels or as input parameters. Orange boxes indicate decaying cohorts, yellow indicate lignin/N contents, green indicate initial cohorts, and purple indicates plant-available N. Large arrows indicate flow of decaying cohort mass.

point they are transferred to either humus (for most litter types) or well-decayed wood (for boles). Cohort decay depends on site conditions (e.g. canopy light level, soil moisture, permafrost depth) and litter characteristics (e.g. initial N and lignin contents, see Table A2). For example, spruce leaf litter has lower initial N concentration and higher initial lignin concentration than does deciduous leaf litter, allowing conifer-dominated sites to have more recalcitrant litter which decomposes more slowly (Flanagan and Van Cleve, 1983; Vance and Chapin, 2001). The annual percent weight loss of each decaying cohort is calculated using a combination of equations from Bonan (1990) and Pastor and Post (1985). If the active layer thickness is shallower than 1.5 m, the average of Eqs. 7 and 8 is used, otherwise only Eq. 8 is used.

$$pM_{loss_B} = f_{LAI}((-0.0052 + 2.08pN)e^{0.898alt}) \tag{7}$$

$$pM_{loss_{PP}} = 0.01f_g\left((0.9804 + 0.09352AET) - \left(\frac{pL}{pN}(-0.4956 + 0.00193AET)\right)\right) \tag{8}$$

where pN and pL are the cohort's current percent N and lignin, respectively, AET is actual evapotranspiration (mm), and f_g and f_{LAI} are decay factors based on light availability and leaf litter which act to increase litter decay with increasing light availability and decreasing leaf litter (Supplementary Material II, Section 4). This percent weight loss is further modified based on a temperature coefficient Q_{10} relationship and a moisture decay factor that acts to decrease percent weight loss with increasing soil moisture and increasing moss depth (Supplementary Material II). Finally, as in Bonan (1990), weight loss of large boles, small boles, well-decayed wood, and twigs are set to 3%, 10%, 5%, and < 20%, respectively.

For all litter types except moss, if the percent remaining of a cohort is less than the critical percent remaining, calculated as $pM_{crit} = 1.7039pL_{init} + 0.0955$, where pL_{init} is the initial percent lignin of the litter cohort (Table A2), the cohort's weight is transferred to either humus or well-decayed wood. For moss litter, the critical weight loss is calculated as the weight loss required for the current N concentration to equal the critical concentration (pN_{crit}, Table A2; Eq. 48 in Supplementary Material II).

If the cohort is not transferred to humus/well-decayed wood, it remains to decay further. The N and lignin concentrations of each decaying cohort are also updated annually as $pN = gN - pN_{crit}pM_{rem}$ and $pL = A - B\frac{M}{M_{init}}$, where pM_{rem} is the percent remaining, M_{init} is the initial mass of the litter cohort (t ha^{-1}), and A and B are input litter parameters (Table A2). The change in N content as a result of decay (δN, tN ha^{-1}) is used to update N immobilization ($\delta N < 0$) and N mineralization each year ($\delta N > 0$).

Humus decomposition occurs similarly to litter decay, using a combination of equations from Pastor and Post (1985) and Bonan (1990) (Eq. 9):

$$pM_{loss} = \begin{cases} f_{most}f_{temp}f_{LAI}((-0.0052 + 2.08pN)e^{0.898alt}), & alt \le 1.5 \\ 0.035f_g f_{moist}f_{temp}, & alt > 1.5 \end{cases} \tag{9}$$

Humus N mineralization ($N_{min_{hum}} = M_N pM_{loss}$) is combined with cohort N mineralization to derive total N mineralization (N_{min}). This value is used to calculate plant-available N (tN ha^{-1}) (Eq. 10):

$$N_{avail} = N_{min} - N_{immob} + N_{fire} + N_{tfall} \tag{10}$$

where N_{immob} is plot-level N immobilization, N_{fire} is volatilized N from fires, and N_{tfall} is N mineralized from throughfall, calculated as 16% of leaf litterfall (Pastor and Post, 1985; Bonan, 1990). The annual organic layer depth (m) is then updated as the combined weights of leaf, twig, and moss litter and humus, divided by cohort-specific bulk density values. See Section 4 in Supplementary Material II for a complete description of the updated soil decomposition routine.

2.2.5. Moss

Moss biomass, depth, and litter amount are also important components of the boreal forest system (Johnstone et al., 2010a). Moss growth can insulate the soil, affecting permafrost depth, and can also impact tree regeneration. A moss growth subroutine was added to UVAFME based on equations from Bonan and Korzukhin (1989). As in their model, moss growth (P, kg m^{-2}) is simulated as the difference between carbon assimilation and respiration (Eq. 11):

$$P = S_\mu M_{biom}A_r - R \tag{11}$$

where S_μ is a specific leaf area parameter, M_{biom} is current moss biomass (kg m^{-2}), A_r is moss assimilation rate (kg kg^{-2}), and R is respiration. Carbon assimilation is assumed to be proportional to maximum moss biomass productivity reported for interior Alaska (μ, 0.2 kg m^{-2}; Van Cleve and Viereck (1981)) and is modified based on plot conditions

such as existing moss biomass, forest floor light level, soil moisture, and forest litter (Eq. 12):

$$A_r = \mu f_{shade} f_{can} f_{decid} f_{moist} f_{ext} \quad (12)$$

where f_{shade} and f_{can} are growth factors relating to light availability, with f_{shade} representing the impacts of shading from the forest canopy on assimilation and acts to decrease A_r at light availability below 50%. The growth factor f_{can} is also based on light availability and acts to simulate the impacts of high light on moss desiccation, acting to decrease A_r at light levels above 50%. The growth factors f_{moist} and f_{decid} are based on soil moisture and deciduous litter amounts, with decreasing soil moisture and increasing deciduous litter leading to lower assimilation rates. Finally, f_{ext} is a light extinction factor which is based on current moss biomass as well as other moss growth and light response parameters (see Section 6, Supplementary Material II).

Respiration is calculated as a function of moss biomass, deciduous litter, soil moisture, as well as other growth parameters (q, b_1, s), and moss litter is calculated based on growth, respiration, and moss growth parameters (Eqs. 13,14):

$$R = S_\mu M_{biom}(q + b_1) + s f_{moist} f_{decid} \quad (13)$$

$$M_{litter} = S_\mu M_{biom}(A_r - q) + s f_{moist} f_{decid} - P \quad (14)$$

The combined depths of the moss and organic layers are additionally used to influence the species-specific regeneration of seedlings, with some species (e.g. black spruce) having a greater capacity to regenerate on a deep moss/organic layer than others (e.g. quaking aspen) (Bonan and Korzukhin, 1989; Johnstone and Kasischke, 2005; Johnstone et al., 2010a) (Eq. 15):

$$f_{org} = \begin{cases} e^{-7.4(d_{org} + d_{moss})}, & tol_{org} = 1 \\ e^{-52.4(d_{org} + d_{moss})}, & tol_{org} \geq 2 \end{cases} \quad (15)$$

where tol_{org} is a species-specific organic/moss-layer regeneration tolerance parameter (1: tolerant; 2: intolerant). This equation was modified from Bonan (1990) using data on post-fire seedling counts from (Johnstone et al., 2010b). Additionally, each species' seedling bank is updated to account for layering and sprouting from species with these abilities. See Section 8 in Supplementary Material II for a complete description of these updates.

2.2.6. Fire

Fire in UVAFME is probabilistic and based on a site-specific fire return interval (FRI). Each year, any individual plot at a site has a probability (i.e. 1/FRI) of burning, independent of other plots (Foster et al., 2017; Shuman et al., 2017). When a fire occurs on a plot, other plots within the site and other sites are unaffected. Previously in UVAFME, fire intensity was also based on an input site-specific mean intensity. Through the explicit tracking of litter type and amount, the existing fire subroutine within UVAFME was modified such that a proxy for fire intensity is calculated based on litter type and amount and soil dryness (Bonan, 1990; Schumacher et al., 2006; Keane et al., 2011). These fire conditions are used to calculate the fire mortality of individual trees as well as to calculate the amount of fire consumption of the litter and humus layers. As with previous versions of UVAFME (Foster et al., 2017; Shuman et al., 2017), probability of fire mortality for each individual tree is based on crown scorch (CS, %) as well as cambial damage, which additionally depends on tree size and bark thickness. In this updated version, crown scorch is calculated based on Schumacher et al. (2006) as (Eq. 16):

$$CS = \begin{cases} 100.0(ck_1 + ck_2 DBH) f_{av}, & DBH < 40 \\ 100.0(ck_1 + ck_2 DBH_{eff}) f_{av}, & DBH \geq 40 \end{cases} \quad (16)$$

where ck_1 and ck_2 are parameters from Schumacher et al. (2006), DBH is diameter at breast height (cm), DBH_{eff} = 40 cm, and f_{av} is the available fuel for burning (t ha^{-1}). Available fuel is calculated as the sum of moss litter, leaf litter, branch litter, and bole litter, each modified by the year's drought index (see Section 7, Supplementary Material II). Fire mortality probability (p_{mfire}) is then calculated as (Schumacher et al., 2006) (Eq. 17):

$$p_{mfire} = \left(1 + e^{-1.466 + 1.91(b_{thick} DBH) - 0.1775(b_{thick} DBH^2) - 0.000541 CS^2}\right)^{-1} \quad (17)$$

where b_{thick} is an input species-specific bark thickness parameter (Table A1). Trees that die by fire are partially consumed, with leaf consumption set to 50%, branch consumption set to 10%, and bole consumption set to 5% (Fahnestock and Agee, 1983; Schumacher et al., 2006). Moss, leaf, branch, and bole litter are consumed according to rates used to calculate f_{av}. As in Bonan (1990), live roots and root litter, well-decayed wood, and humus are additionally consumed based on soil dryness and moss-organic layer depths (Supplementary Material II). For all biomass burned by fire, some proportion of N is volatilized (pN_{vol}) and made available to plants based on soil dryness and moss-organic layer depth (Bonan, 1990):

$$pN_{vol} = 1 - \max(0.0, \min(0.6426 DI + 3.34(d_{moss} + d_{org})), 0.7) \quad (18)$$

where DI is an annual drought index calculated as the proportion of the growing season where daily $\frac{w_l}{m_{fc}} < 0.75$. Volatilized N is then calculated as $N_{fire} = M_{cons} pN_{vol} pN$, where M_{cons} is the mass consumed by fire, and pN is the N concentration of the litter. See Section 7 of Supplementary Material II for a complete description of these updates.

Following code updates, we tested these modifications against existing site-level observations of solar radiation, evapotranspiration, permafrost depth, soil moisture, organic layer depth, and snowpack depth at locations across interior Alaska (see Supplementary Material II). These tests showed that the model could accurately produce important abiotic drivers within the study region, at both annual and daily scales and across a distribution of sites with varying climate, topographic, and soil conditions.

2.3. Study area and forest inventory validation sites

Our study area is defined by the boreal forests within the Tanana River Basin of interior Alaska (AK) (Fig. 4), as this watershed encompasses most of the field sites used to test the model in this study. The Tanana River Basin is bordered by the Alaska Range to the south and the Mackenzie Range to the east. It consists primarily of lowland forests of black spruce on poorly drained soils, white spruce in well-drained areas, and upland forests of paper birch and quaking aspen (Chapin et al., 2006b; Andersen et al., 2011). Mean annual temperatures vary between −19 °C and −1 °C, with a mean of about −3 °C. Annual precipitation varies between 225 mm in the eastern valley and 2800 mm at the highest elevations, with a mean of about 550 mm, and with about 35% falling as snow (Yarie et al., 1998; Wang et al., 2016).

Inputs to UVAFME include climate (monthly temperature minima and maxima, precipitation, and cloud cover); site characteristics such as topography and mean fire probability; and soil characteristics such as drainage type and soil texture. Site and climate parameters were derived for 244 testing and forest inventory sites as well as for 28,503 sites within the Tanana River Basin on a 2 km grid. Historical temperature and precipitation distributions for these site locations were obtained from ClimateNA v5.50 software (Wang et al., 2016). Historical cloud cover distributions were obtained from the Climatic Research Unit (CRU) TS 3.26 dataset (Harris et al., 2014).

Topographic input data (i.e. elevation, slope, and aspect) for each site were obtained from a 1 km digital elevation model downscaled from GTOPO30 data (Lindgren and Kurkowski, 2012). At the individual sites, soil characteristics (i.e. saturation capacity, field capacity, and soil texture) were obtained from detailed site descriptions and available data on soil texture and drainage conditions (Yarie, 1998; Vogel, 2007; Ruess, 2015). At the 28,503 gridded sites, these soil characteristics were derived via topography and maps of soil texture from SoilGrids and

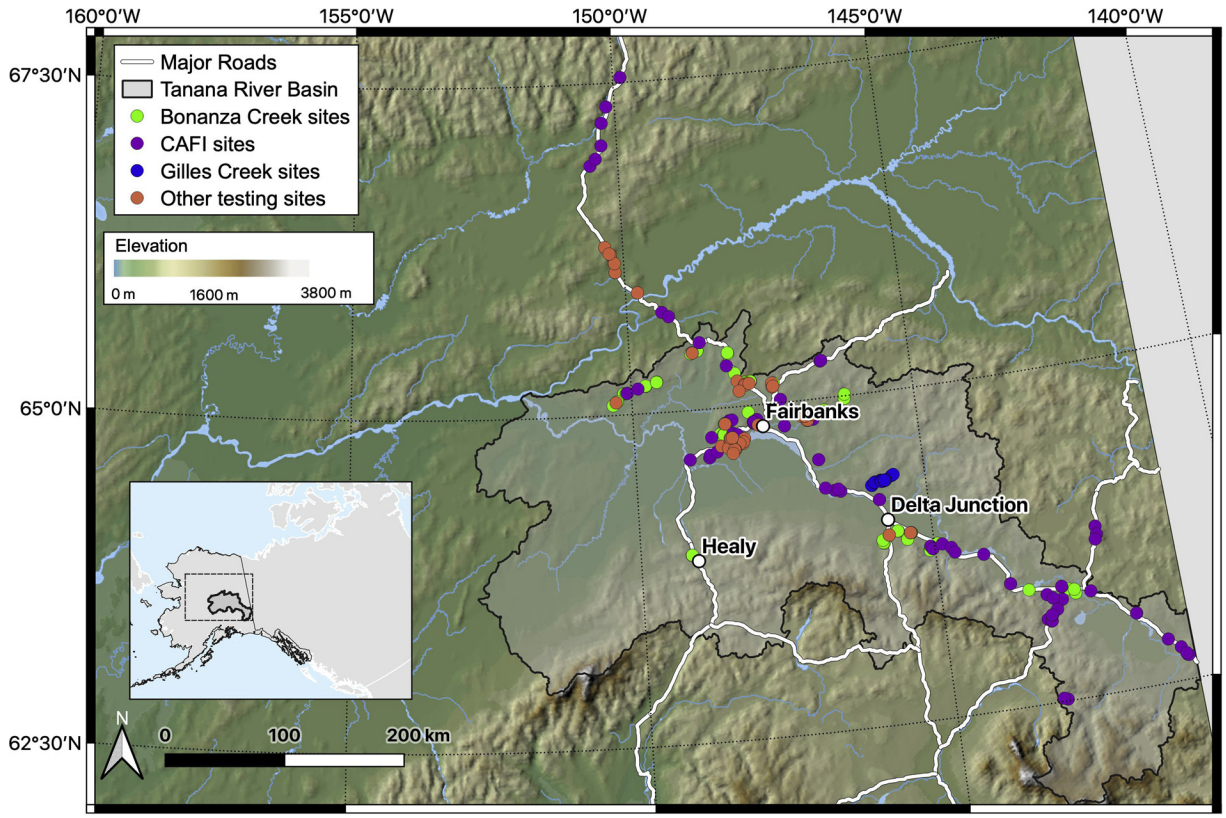

Fig. 4. Study area and individual testing sites. Orange testing sites were used to test success of model updates against observed data for soil moisture, permafrost depth, evapotranspiration, solar radiation, organic layer depth, and snow pack depth (see Supplementary Material II). Bonanza Creek, CAFI, and Gilles Creek sites were used to validate model output on forest characteristics with inventory data.

active layer thickness from the Alaska LandCarbon Project (see Supplementary Material I). Input mean FRI was calculated using fire probability maps from ALFRESCO model outputs simulated under historical climate (Bennett et al., 2017) (Supplementary Material I).

Input species characteristics for UVAFME include average maximum diameter, height, and age, as well as tolerances to environmental and climate conditions (Table A1). Such input values do not change between simulated sites, and thus represent average species characteristics for a simulated domain. These input characteristics for the seven main tree species of interior Alaska (i.e. *Betula kenaica*, *B. neoalaskana*, *Larix laricina*, *Picea glauca*, *P. mariana*, *Populus balsamifera*, and *P. tremuloides*) were determined based on information in the scientific literature (Botkin et al., 1972; Burns and Honkala, 1990; Nikolov and Helmisaari, 1992; Chapin et al., 2006a; Viereck and Little, 2007; Keane et al., 2011). Species range maps were obtained from Viereck and Little (2007) and used to determine which species were eligible for colonization and growth at each site (Supplementary Material I).

To assess the ability of the updated version of UVAFME to accurately simulate forest dynamics within interior Alaska, model output was compared to forest inventory datasets within the region (Fig. 4). The Cooperative Forest Alaska Inventory (CAFI) dataset contains 227 ~405 m^2 permanent sample plots (PSPs) on 77 sites within interior Alaska (initial sampling date in 1994), all of which have been resampled once, and many of which have been resampled two and three times (61% and 42%, respectively) (Malone et al., 2009). The individual PSPs represent replicate plots for the sites, with each site typically containing three PSPs spaced 30–63 m apart. Most of the locations are comprised of mature stands of white spruce (*P. glauca*; 41% of total biomass across all sites), Alaska birch (*B. neoalaskana*; 31%), and quaking aspen (*P. tremuloides*; 19%), with some black spruce (*P. mariana*; 6%), balsam poplar (*P. balsamifera*; 3%), and Tamarack (*L. laricina*; < 0.01%) (Fig. A4).

The 67 Bonanza Creek sites (Fig. 4) are from the Bonanza Creek Long Term Ecological Research Station's extended site network. Between 2008 and 2011, these sites were surveyed to study post-fire successional pathways and above- and belowground C and N pools (Alexander et al., 2012; Alexander and Mack, 2015). Within each site five 20 m sub-transects along a 100 m transect were established, and within a 5–10 m portion of each transect the DBH of trees taller than 1.4 m and the basal diameter for trees < 1.4 m were measured within a 1 m section on either side of each sub-transect (Alexander and Mack, 2015). Most of the sites consist of Alaska birch (55% of total biomass across all sites), quaking aspen (27%), and black spruce (15%), with some white spruce (3%), balsam poplar (0.3%), and Tamarack (0.05%) (Fig. A5).

The 30 Gilles Creek sites (Fig. 4) were sampled for studies focusing on the effects of wildfires on carbon budgets (Rogers et al., 2014) and microbial communities (Holden et al. 2016). The sites comprised 22 stands which burned in the 2010 Gilles Creek fire (64°20′N, 145°45′W), and eight which did not burn. Species and DBH were recorded for every tree inside a 2 m × 30 m transect within each site in late August 2012. In the burned plots, pre-fire conditions were estimated using the DBH and species of burned trees, as is common in wildfire studies (e.g. Boby et al., 2010; Rogers et al., 2014). The sites were dominated by black spruce (50% of total biomass across all sites) and white spruce (39%), with some quaking aspen (11%) and Alaska birch (< 1%) (Fig. A6).

For comparison with UVAFME, the raw CAFI and Gilles Creek inventory data were processed as in Rogers et al. (2018). Only simulated and inventory trees greater than 0.5 cm DBH (for Gilles Creek) and 3.8 cm (for the CAFI dataset) were considered to account for the minimum tree size measured in the inventory data. Aboveground dry biomass (kg) was calculated for each measured tree using allometric relationships from Alexander et al. (2012) (for white spruce ≥ 3.7 cm DBH; balsam poplar ≥ 4.1 cm DBH; and Alaska birch, quaking aspen,

and black spruce), Ung et al. (2008) (for white spruce and quaking aspen), and Lambert et al. (2005) (for balsam poplar and Tamarack). For each tree, if multiple allometric relationships were applicable, the average biomass from the relevant equations was used (Rogers et al., 2018). The relevant allometric equations were chosen for each tree species and tree size based on the philosophy within Rogers et al. (2018, 2014), where the available equations for each tree species were assessed for their biases, consistencies, and representativeness (i.e. number of samples and geographic location).

For the CAFI sites, total species-specific biomass was summed for each PSP and then averaged across PSPs for each site. For the Gilles Creek sites, total species-specific biomass was summed for each site. Total stem density (trees ha^{-1}) was also determined for the Gilles Creek sites. The Gilles Creek sites were also grouped into white spruce- and black spruce-dominated stands as in Rogers et al. (2014) to calculate average species-specific biomass and stem density for the two different site types. For the Bonanza Creek sites, aboveground biomass for each tree was calculated via allometric equations from Bond-Lamberty et al. (2002) and Yarie et al. (2007) (see Alexander et al., 2012). Average stand-level biomass was then calculated for each species on each of the sites.

Tree cores had been taken between 2009 and 2011 at 32 of the CAFI sites, with between two and six tree cores per site (mean of four) (J. Yarie, *unpublished data*). Stand ages for these sites were estimated using the age of the oldest tree cored as in Johnstone and Kasischke (2005). Stand age was also estimated from plot-scale information and fire history polygons from the Alaska Large Fire Database (Kasischke et al., 2002) where the polygons intersected with the CAFI plots. Tree cores were also taken from a random sample of 10 trees at each Bonanza Creek site. These cores were used to estimate the stand age of each site as the average of the ring counts of the 10 cores (Alexander and Mack, 2015). No stand age information was available for the Gilles Creek sites.

2.4. Model calibration and validation

During an initial calibration phase, UVAFME was applied at 14 CAFI inventory sites where stand age was known based on the available tree core data. We ran UVAFME from bare-ground initiation to the estimated stand age, and compared modeled species-specific biomass to inventory data. Input species characteristics were modified to maximize agreement between the model output and the inventory data, while maintaining realistic values for the input species parameters based on the previous literature review (Burns and Honkala, 1990; Nikolov and Helmisaari, 1992; Chapin et al., 2006a; Viereck and Little, 2007).

Following this calibration phase, UVAFME output on species-specific biomass (tC ha^{-1}) was compared to the CAFI (at the first sampling date), Bonanza Creek, and Gilles Creek sites, which included the 14 calibration sites as well as 160 independent validation sites. Where a stand age estimate was available, model output at that age was used to compare to the inventory data, and otherwise model output at year 200 was used. At individual inventory sites, the variance in species-specific biomass within each site (i.e. across the site-specific PSPs/sub-transects/site types) was quite high (average coefficient of variation of biomass ranged from 0.90 to 1.75, Fig. A7), likely due to the low sample size (typically three to five PSPs/sub-transects) and the heterogeneity of the interior Alaskan landscape. At a local scale (i.e. $< 500\ m^2$), forest conditions are impacted by land history and stochastic factors such as seed rain, treefall, herbivory, and other random events (Shugart, 1984; Bugmann et al., 1996). Although UVAFME does incorporate stochasticity into the mortality and regeneration processes, land history, human disturbance, and specific stochastic events and their fine-scale repercussions cannot be predicted on an individual basis (Keane et al., 2001; Hurtt et al., 2016). Thus, the landscape-scale output from gap models like UVAFME (i.e. the average of several hundred simulated plots at a site) represents average expected forested conditions over time, similar to an average of a large sampling of replicate forest inventory plots (Bugmann et al., 1996). We therefore compared average species-specific biomass across all inventory sites to average model-simulated biomass, rather than comparing biomass on a site-by-site basis. Additionally, to determine if UVAFME could accurately represent different forest types within Alaska, we compared average model output at the Gilles Creek sites to average measured conditions at the black spruce and white spruce site types.

To account for the lack of site-to-site comparisons, we additionally ran an initialization comparison test at the CAFI sites where multiple remeasurements were available. We first initialized the model to the first sample date of each individual CAFI site using site-specific distributions of tree species and site- and species-specific distributions of stand structure (trees DBH size $class^{-1}$) derived from the CAFI data (sample year 0). Model output was then compared to subsequent CAFI remeasurements on a site-by-site basis. This allowed us to incorporate land history effects on species composition and size structure, while also testing UVAFME's prediction of forest dynamics over time.

2.5. Climate change application

Following these model tests, we performed a climate change application to predict how forests of interior Alaska are likely to change in coming decades. Future climate data (mean monthly temperature and precipitation) were obtained from a 771 m resolution CMIP 5 five-model average for the RCP 4.5 and 8.5 scenarios (Leonawicz et al., 2015a, 2015b). This climate change prediction covered years 2006 to 2100 and resulted in an average increase in temperatures of about 2.6 °C (RCP 4.5) and 5.9 °C (RCP 8.5) and an increase in precipitation of about 119 mm (RCP 4.5) and 166 mm (RCP 8.5) (Fig. A8) for the Tanana Valley and the inventory sites. For this application we ran UVAFME at the inventory sites as well as across the Tanana River Basin in a gridded, wall-to-wall fashion at 2 km grid cell resolution (n = 28,503). At each site, we simulated UVAFME from bare ground initiation (each with 200 plots each at 500 m^2) to the estimated stand age in 2006 (or to year 200 if no stand age information was available), and subsequently initiated the climate change application.

3. Results

3.1. Model performance at inventory sites

UVAFME performed well at predicting species-specific biomass across the inventory sites (Fig. 5) and at the black spruce- and white spruce-dominated Gilles Creek sites (Fig. 6, A9). Across the inventory sites, UVAFME predicted mostly white spruce (*Picea glauca*) and Alaska (AK) birch (*Betula neoalaskana*), a moderate amount of quaking aspen (*Populus tremuloides*) and black spruce (*Picea mariana*), and some balsam poplar (*Populus balsamifera*). UVAFME slightly overpredicted black spruce and balsam poplar biomass at these sites, though still accurately represented relative species dominance. The root mean square error across all species-specific biomass was 12.17 tC ha^{-1} and t-tests showed significant differences ($p < 0.05$) between inventory- and model-derived biomass of Kenai birch (difference = 0.99 tC ha^{-1}), Tamarack (difference = 0.054 tC ha^{-1}), black spruce (difference = 2.83 tC ha^{-1}), and balsam poplar (difference = 2.51 tC ha^{-1}).

Before updates were made to the model (Section 2.2), UVAFME could not accurately differentiate between the black and white spruce site types at the Gilles Creek locations (Fig. A1; A2). However, following the addition of soil-vegetation-wildfire feedbacks, the model was able to accurately predict forest succession and vegetation composition at black spruce and white spruce site types. At the eight white spruce-dominated Gilles Creek sites, UVAFME predicted higher biomass of white spruce, with lower biomass of AK birch, quaking aspen, and black spruce, comparable to the inventory data, though with a fairly high RMSE (Fig. 6; RMSE = 21.48 tC ha^{-1}). However, t-tests across all species only showed significant differences between inventory and

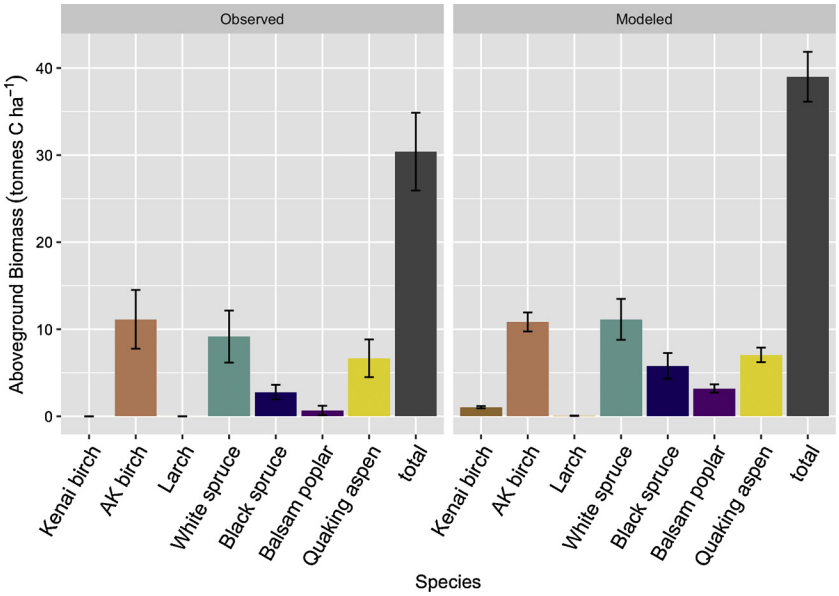

Fig. 5. Model output on species-specific aboveground biomass (tC ha^{-1}) averaged across all 174 inventory sites within interior Alaska (Fig. 4) compared to inventory-derived biomass. Error bars indicate 95% confidence intervals.

model-simulated biomass of AK birch ($p < 0.001$; difference = 4.84 tC ha^{-1}). UVAFME output on stem density at the eight Gilles Creek white spruce sites was also comparable to the inventory measurements, though with some variation, showing higher black spruce stem density and lower white spruce stem density (RMSE = 1307 stems ha^{-1}) than was measured. T-tests did show significant differences between modeled and measured stem density for white spruce ($p = 0.037$; difference = -1532 stems ha^{-1}) and AK birch ($p < 0.001$; difference = 717 stems ha^{-1}).

At the 22 black spruce dominant Gilles Creek sites, UVAFME output on species-specific biomass was comparable to inventory-derived biomass (Fig. A9) (RMSE = 6.14 tC ha^{-1}), with a slight but statistically significant overprediction of white spruce biomass ($p = 0.0022$; difference = 6.6 tC ha^{-1}). UVAFME output on species-specific stem density at the Gilles Creek black spruce sites (Fig. A9) was overall comparable to the inventory data, showing a high density of black spruce

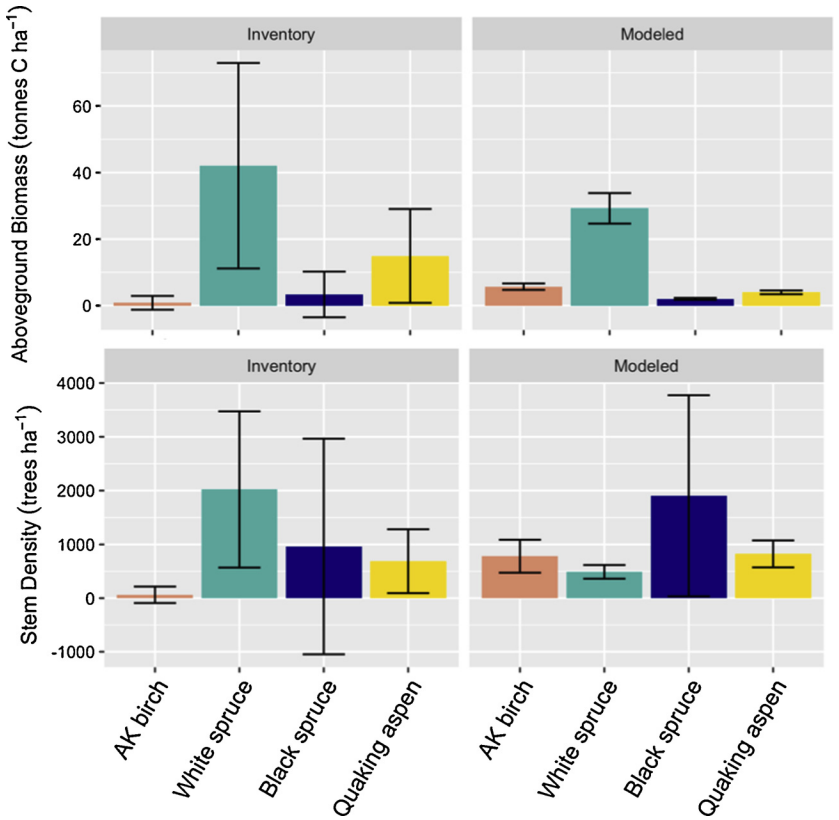

Fig. 6. Model output on species-specific aboveground biomass (tC ha^{-1}) (top) and stem density (stems ha^{-1}) (bottom) averaged across eight white spruce-dominated Gilles Creek sites (Fig. 4) compared to inventory-derived biomass and stem density. Error bars indicate 95% confidence intervals.

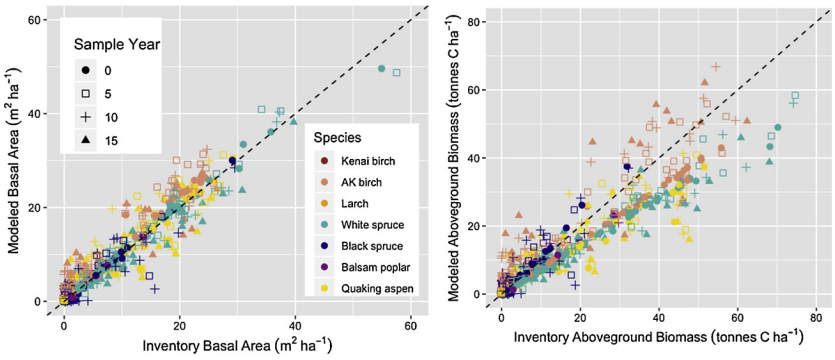

Fig. 7. Model output on species-specific basal area ($m^2\ ha^{-1}$) and biomass (tC ha^{-1}) at 77 CAFI sites, with each site/sample year represented by one point, compared to inventory data. UVAFME was initialized to the first sampling date (closed circles: sample year 0) and subsequently compared to following CAFI remeasurements (open squares: sample year 5; crosses: sample year 10; closed triangles: sample year 15). The dashed line corresponds to perfect prediction of measured basal area/biomass (i.e. the 1:1 line).

stems, and a very low density of all other species' stems. The RMSE was fairly high, however, at 2452 stems ha^{-1}, and t-tests showed significant differences between black spruce stem density ($p = 0.027$; difference = -2131 stems ha^{-1}) and AK birch stem density ($p = 0.025$; difference = 68 stems ha^{-1}). In general, however, UVAFME predicted a very high number of black spruce stems at the black spruce site types (Fig. A9) and more moderate numbers of stems overall at the white spruce site types (Fig. 6), which is comparable to the inventory measurements at those locations, as well as to descriptions of black and white spruce-dominated forest stands within the region (Viereck et al., 1983).

When initialized to the first CAFI sampling date, UVAFME predicted subsequent remeasurements of species-specific biomass (RMSE = 5.33 tC ha^{-1}) and basal area (RMSE = 1.82 $m^2\ ha^{-1}$) with high accuracy (Fig. 7), though predicted biomass less well, especially white spruce biomass. Site-level comparisons with initialized UVAFME output and subsequent CAFI resampling (e.g. site 1003; Fig. A10) showed that UVAFME was able to predict species-specific biomass dynamics over time. These results indicate that the model is able to accurately represent the successional dynamics over time across a wide variety of sites, as a result of individual tree interactions with the environment as well as tree-tree competition.

3.2. Climate change

With increasing temperatures and precipitation, UVAFME predicted changes in biomass and species composition, both at the inventory locations (Fig. 8) and across the Tanana River Basin (Figs. 9 and 10) for both climate change scenarios, with RCP 8.5 resulting in more extreme change. At a broad scale, UVAFME predicted decreases in biomass (particularly for spruce) in dryer, interior sites (Fig. 9, A11–A14), with a shift towards higher deciduous fraction (Fig. 10). In contrast, UVAFME predicted increases in biomass at wetter, colder sites as well as at high elevation sites.

These changes in biomass and species composition coincided with increases in atmospheric demand (for RCP 8.5) (Fig. A17), soil dryness (for both RCP scenarios) (Fig. A18), and decreases in soil organic C (Fig. A19). UVAFME also predicted a shift in the main growth-limiting factor from mainly shade and low temperature stress prior to climate change (Fig. A20) to mainly drought and nutrient stress following climate change (Fig. A21, A22). Under extreme climate change (i.e. RCP 8.5), drought stress was the main growth stress for most trees (Fig. A22), however under more moderate climate change (i.e. RCP 4.5) nutrient and drought stress increased for trees over 10 m in height (Fig. A21). These areas of elevated nutrient stress occurred in areas with declining biomass (Fig. 9), indicating that at more moderate levels of temperature increases, tree-tree competition for nutrients or other resources may play a major role in driving forest change.

At a local scale, forest response to climate change depended on site conditions such as soil moisture, active layer depth, and organic layer depth, as well as species composition (Fig. A23–A30). For example, at pre-climate change black spruce sites, soil moisture tended to be high and active layer depth was fairly shallow (Fig. A24; A25), as is typical for this forest type (Viereck et al., 1983). At these sites, the main stressor on black spruce trees was cold temperatures and, to a lesser extent, low moisture stress (Fig. A26). Once temperatures increased, cold temperatures were no longer a major stressor for black spruce trees, and stress from low moisture also decreased due to increases in precipitation and previously frozen water released from thawing permafrost. These site and soil changes resulted in an increase in the growth rate of black spruce individuals and subsequently an increase in overall biomass (Fig. A11; A12; A24). Thus, at these sites, increases in moisture from precipitation and thawing permafrost were able to outpace the increases in temperature and evaporative demand.

At dryer, white spruce-dominated sites, active layer depth was already quite high (i.e. > 1 m) and soils were moderately dry (Fig. A27; A28) under historical conditions. At these sites, the main stressors were

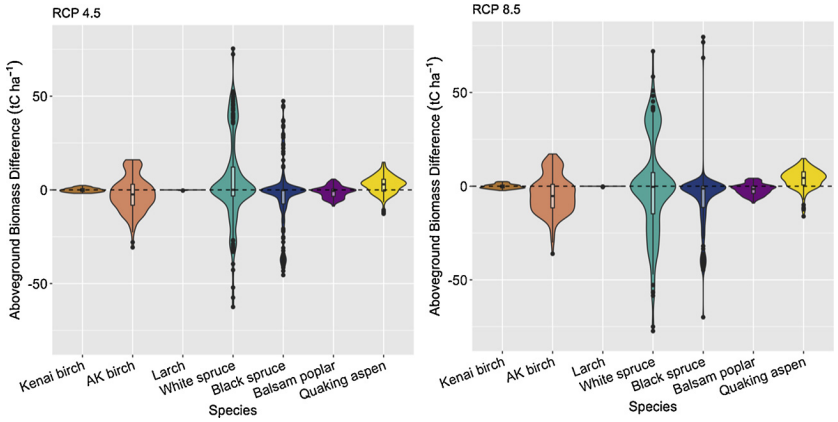

Fig. 8. Model output on species-specific biomass difference (post- minus pre-climate change) density plots (tC ha^{-1}) at the Bonanza Creek, CAFI, and Gilles Creek sites (n = 174; Fig. 4) between pre- and post-climate change values for RCP 4.5 (left) and RCP 8.5 (right) climate scenarios.

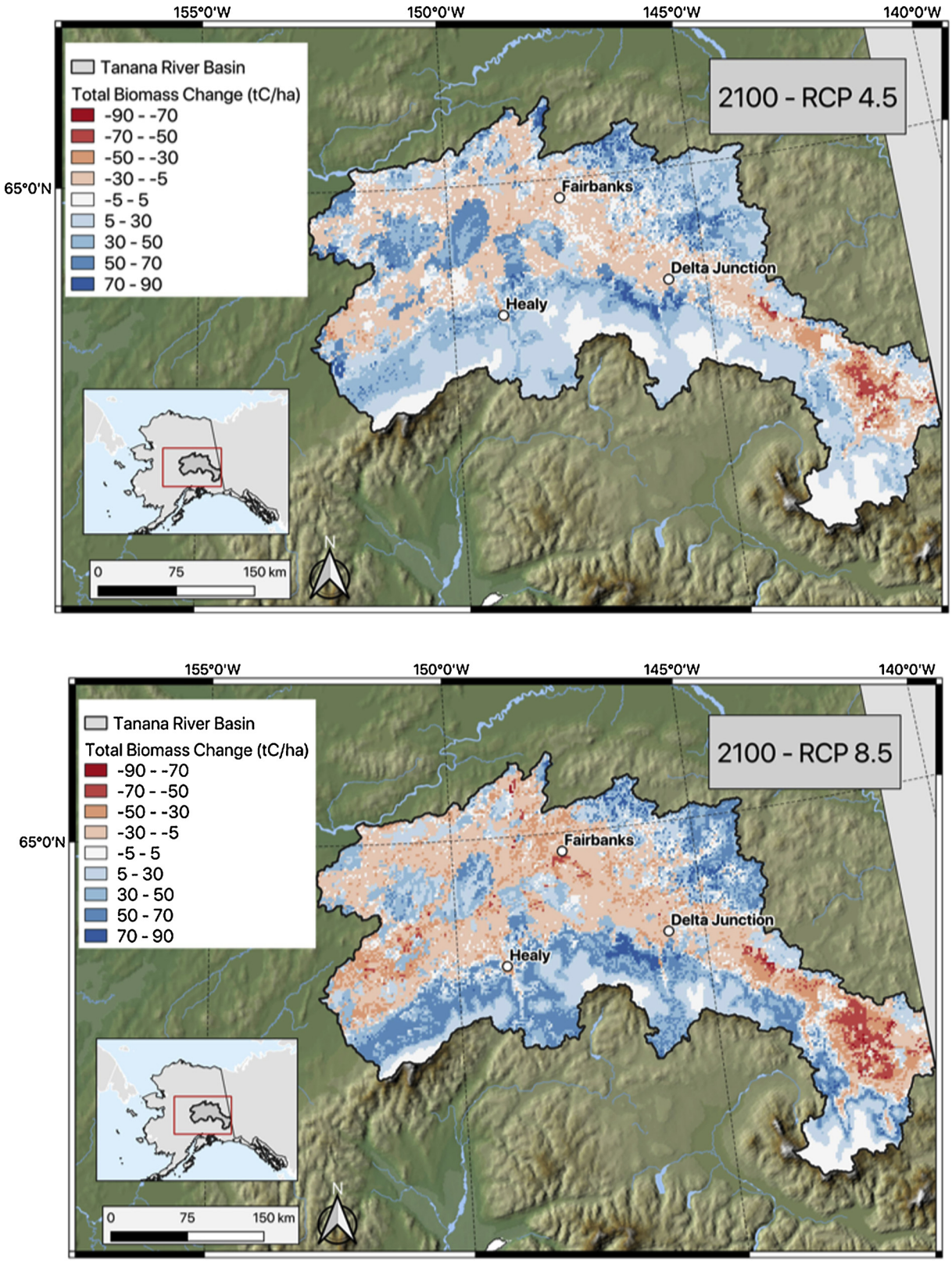

Fig. 9. Model output on total biomass difference (post minus pre-climate change; tC ha^{-1}) across the Tanana Valley (2 km grid cell resolution) between pre- and post-climate change conditions for RCP 4.5 (top) and RCP 8.5 (bottom) climate change scenarios.

already low soil moisture and low nutrients (Fig. A29). Thus, when climate change occurred, increasing temperatures only acted to further increase drought stress via increasing evaporative demand, and thus mortality of white spruce and birch eventually occurred (Fig. A27; A29). At many of these sites, the trajectories were not linear (Fig. A27; A30). Some, such as in white-spruce dominated and mixed white spruce/black spruce sites, saw increases in spruce and birch biomass initially, as increasing temperatures resulted in increasing vegetation

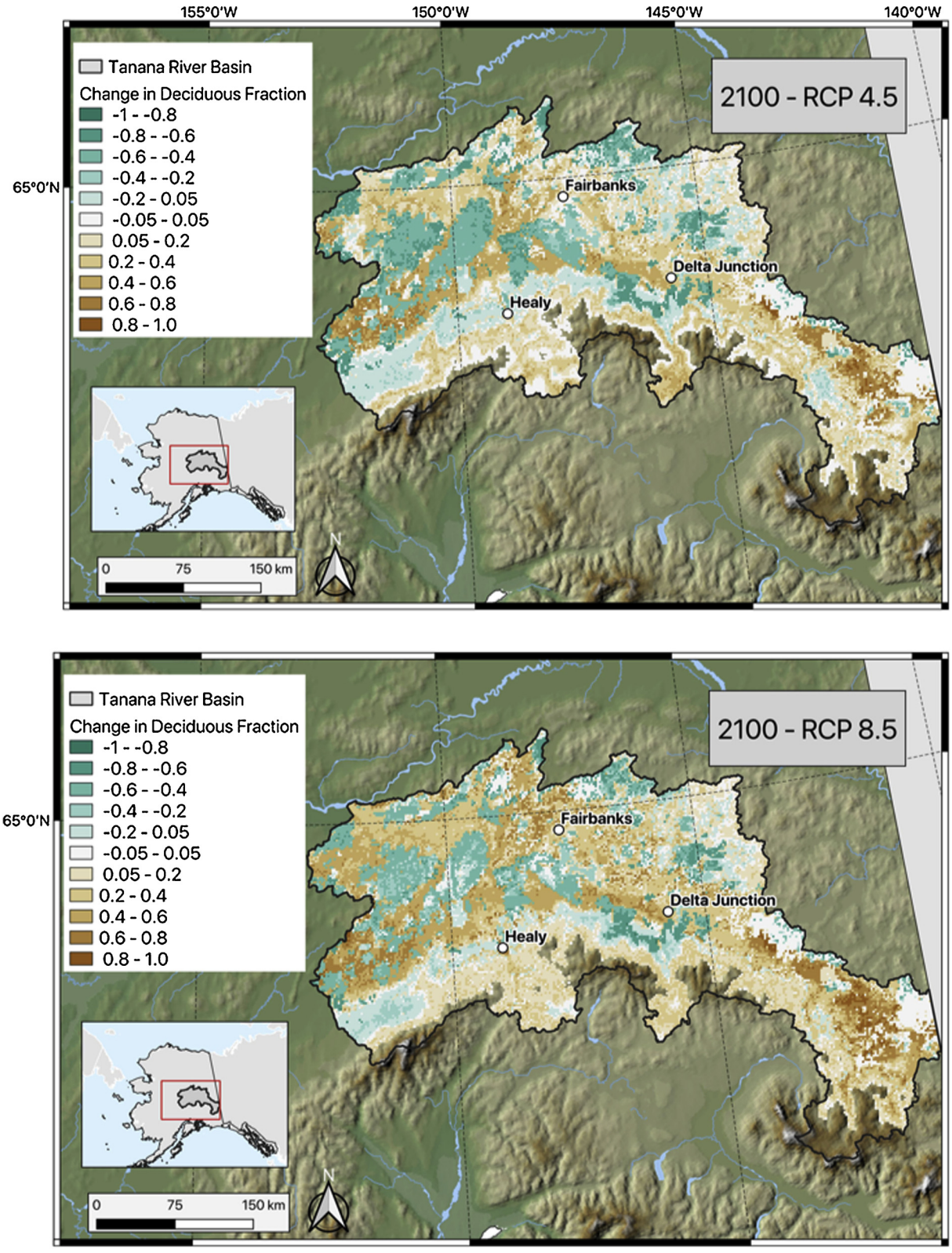

Fig. 10. Model output on deciduous fraction (0–1) difference (post minus pre-climate change) across the Tanana Valley (2 km grid cell resolution) between pre- and post-climate change conditions for RCP 4.5 (top) and 8.5 (bottom) climate change scenarios.

productivity. However, eventually the increases in evaporative demand and decreases in soil moisture caused decreasing productivity under both scenarios and the eventual mortality of these more drought intolerant species under the RCP 8.5 scenario (Burns and Honkala, 1990; Nikolov and Helmisaari, 1992). This shift in biomass trajectories indicates a potential threshold for temperature rise after which moisture stress becomes predominant. In contrast, quaking aspen, a characteristically drought tolerant species, was able to grow and thrive in the gaps created by the dying birch and spruce (Fig. A15; A16; A27; A30).

4. Discussion

4.1. Model validation

It is clear based on previous field- and modeling-based studies that interactions between climate, vegetation, soils, and wildfire, and any potential future changes to these drivers, are crucial components to include in predictions of future forest state in the boreal zone (Camill et al., 2001; Hogg et al., 2008; Trugman et al., 2017; Fisher et al., 2018; Rogers et al., 2018). Indeed, it was only until all code updates were finalized that UVAFME was able to accurately simulate forest dynamics and characteristics within interior Alaska (Fig. A1; A2). Even intermediate testing between major updates (e.g. after permafrost/soil water updates but before soil nutrient and fire updates) still resulted in poor agreement with inventory measurements and expected successional pathways. Once incorporated into the model, however, detailed interactions between vegetation, soil characteristics, and wildfire at the stand- and tree-level (Fig. A31) lead to realistic successional dynamics and forest characteristics, and improved model comparisons to data on forest characteristics (Figs. 5–7; A9) and abiotic drivers (Supplementary Material II).

Some slight, though statistically significant, dissimilarities did arise between inventory data and UVAFME output (Fig. 5,6; A9), though this existed primarily where the species' biomass/stem density was low and variability was high. In general, the inventory-measured stem density was quite variable, with species-specific standard errors ranging from 0.24 to 2.3 times the mean species-specific stem density, thus lowering the statistical power of these comparisons (overall Type II error was 93% for the white spruce and 38% for the black spruce site stem density comparisons). This high variability is skewed towards the smaller stems (e.g. mean ± SE stem density of measured black spruce trees between 0.5 and 5 cm DBH at the black spruce sites was 4179 ± 1848 stems ha^{-1}), as a result of the stochastic nature of regeneration and mortality of young trees (Shugart, 1984; Shugart et al., 2018). Regeneration and survival of small stems in interior Alaska is influenced by the temporal cycle of seed production (Zasada et al., 1992), fire history (Johnstone and Kasischke, 2005), soil characteristics (Johnstone et al., 2010a; Alexander and Mack, 2015), and browsing by hares and other animals (Olnes and Kielland, 2016). UVAFME does include deterministic and stochastic processes to simulate these factors (Foster et al., 2017; Yan and Shugart, 2005). However, at a very local scale (i.e. with only an average of 8–22 sites), it is not possible to simulate the exact events that lead to the specific number of small stems at a specific location (Shugart, 1984; Hurtt et al., 2016).

Additional differences may have occurred due to discrepancies in the input versus the actual FRI. Site-level fire probability is a site-specific input parameter, based on outputs from the ALFRESCO model (Bennett et al., 2017). Though in this updated model fire intensity does depend on fuel conditions and moisture, and fire probability is tied to climate via an aridity index (Foster et al., 2018), fire occurrence does not interact with site-level fuel characteristics (i.e. moisture content, geometry, flammability, etc. (Rothermel, 1972)). This potential mismatch between input and actual fire probability would have impacted the mortality and regeneration processes at each site, as vegetation dynamics and deciduous fraction are tightly linked to wildfire and fuels consumption (Fig. A31) (Johnstone et al., 2010b; Bernier et al., 2016), thus leading to slightly differing biomass and stem density between modeled and actual values. Future work with UVAFME will include prognostic fire occurrence based on fire weather and fuel conditions (rather than based on input probabilities).

The moderate differences between modeled and observed white spruce biomass (but not basal area) for the initialization test, even at year 0 when trees were first initialized (Fig. 7), may be due to the different methods of estimating biomass. While the inventory biomass measurements were based on allometric equations only using tree DBH, UVAFME uses DBH, height, and canopy depth to estimate biomass (Yan and Shugart, 2005). Because canopy depth in UVAFME is not calculated allometrically, but rather decreased based on tree stress throughout its lifetime (i.e. via lower branch thinning), initialized trees are given a default value of canopy depth as 30% of initialized tree height, as in Thonicke et al. (2010). This use of a default value when initializing may give rise to discrepancies between inventory and model-estimated biomass as opposed to when trees are simulated from bare ground regeneration. Future work with UVAFME will include initialization to current stand conditions via high-resolution LiDAR data (Foster et al., 2019) which will give estimates of current tree height as well as canopy depth (Wasser et al., 2013), alleviating some of these discrepancies.

UVAFME's ability to reliably predict site and forest characteristics at a local scale when confronted with various types of inventory and field data increases confidence in its predictions of forest-climate-soils interactions under current and future climate scenarios. These interactions, which are principal drivers of forest dynamics and characteristics within interior Alaska (Johnstone et al., 2010a), are able to be simulated in a fine-scale, process-based manner due to the tree- and species-level resolution of UVAFME. Without such fine-scale connectivity, the individual tree interactions with surrounding trees and their environment cannot be completely represented, and important biotic-abiotic interactions are not captured (Fig. A1; A2). In the North American boreal zone, where such biotic-abiotic feedbacks are integral to ecosystem dynamics, it is even more crucial that such interactions are included in modeling endeavors within the region.

Additionally, following modification of species-level parameters based on initial results at the 14 calibration sites (see Section 2.4), UVAFME was not "tuned" to specific site, climate, or stand conditions. The model was thus able to reproduce accurate local- and regional-scale vegetation and site/soil characteristics with a fairly general parameterization scheme and only a moderate number of parameters. Such broad applicability of UVAFME combined with its fine-scale (i.e. tree-level) detail make it ideal for application across large regions with important multi-scale drivers and interactions.

4.2. Forest response to climate change

The future biomass and species composition trajectories predicted by UVAFME agree with other broader scale modeling studies in this region. For example, the state-transition/ecosystem model ALFRESCO-TEM similarly predicted overall decreases in spruce forests and increases in deciduous forests (Euskirchen et al., 2016) (Fig. 8; A11-A16) as well as local increases in biomass and coverage of spruce forests with increasing growing season length near cold range boundaries (Euskirchen et al., 2009) (Fig. 9). These results also agree with a recent modeling study using *ecosys* (Mekonnen et al., 2019), a broad-scale ecosystem model, which found that nutrient dynamics along with precipitation and fire regime changes were key driving factors of increasing deciduous fraction across Alaska under an RCP 8.5 climate change scenario. UVAFME results highlight the importance of fine-scale interactions between site and soil characteristics (Fig. A23–A30; A32). The response of individual trees and individual stands to climate change in these simulations was dependent not only on pre-climate change conditions, but also on the ongoing successional and competitive dynamics during the climate change application. Following mortality of drought-intolerant spruce trees at interior/drier sites (Fig. A11–A14; A27; A30) from increasing evaporative demand (A17), declining soil moisture (A18), and subsequently increasing drought stress (A21; A22; A29) the more drought tolerant and faster growing deciduous species (e.g. AK birch and quaking aspen) (Burns and Honkala, 1990; Chapin et al., 2006a) were able to grow and reproduce successfully in the gaps created by the dying spruce trees (Fig. A16; A29). Under the RCP 8.5 scenario, shade stress for AK birch and quaking aspen at these sites decreased, indicating that these trees were "released" from competition as the spruce trees died (Fig. A29). In addition, these results show that under moderate temperature increases (i.e.

RCP 4.5), tree-tree competition for light and nutrients, along with drought stress, may be a main cause for future tree mortality and species shifts in Alaska (Fig. A21), as these resource-dependent stressors became more important as climate change progressed. Such changes in species composition due to shifting environmental conditions were furthered through feedbacks to soil conditions (Fig. A32). Following increases in deciduous fraction, litter decay occurred more rapidly due to the shift towards deciduous (rather than recalcitrant spruce) litter, resulting in a decrease in the soil organic layer, an increase in the active layer, and an increase in plant-available N (Fig. A32). Thus, the demographic changes predicted by UVAFME fed back to the soil-vegetation system, leading to lasting changes in vegetation type. Rather than models that represent plants as groups of vegetation (i.e. PFTs), a model like UVAFME, which can simulate these interactions at their inherent scale (i.e. individual trees/species), is able to represent in detail the structural and demographic changes associated with changing environmental and climate conditions. Such changes have the capacity to influence further climate change through evapotranspiration, albedo, surface roughness, and other biophysical feedbacks (Liu et al., 2006; Beck et al., 2011a). Thus, it is important for global land surface models to consider the implications of simulating plants at only a broad, PFT/"big leaf" scale.

The initial increase and eventual decrease in spruce biomass in some areas predicted by UVAFME (Fig. A27; A30) is also comparable to results from ALFRESCO-TEM simulations for interior AK (Zhu and McGuire, 2016), which predicted increases in spruce forest area until about 2080, after which sharp declines occur under the A2 climate scenario (climate forcing from the Canadian Centre for Climate Modelling and Analysis' Coupled Global Climate Model; CGCM3.1). In contrast, the same simulation with A2 climate forcing from the ECHAM5 (the Max Planck Institute's European Center Hamburg Model) model, which predicted greater temperature increases and smaller precipitation increases compared to the CGCM model as well as to the GCM forcing used in our study, showed spruce declines throughout the 2020–2100 time period. These results suggest that there is likely a tipping point for increasing temperatures after which the higher atmospheric demand and drying soils outstrip the potential benefits from increased productivity, and competition for nutrients, light, and moisture with more drought-tolerant, faster-growing species increases (Fig. A29; A32) (Juday et al., 2015).

Climate change results from UVAFME are also in agreement with trends predicted by recent remote sensing, forest inventory, and dendrochronology studies in Alaska (Beck et al., 2011b; Juday et al., 2015; Ju and Masek, 2016; Trugman et al., 2017; Pastick et al., 2019). Remote sensing and dendrochronology records show increasing productivity in cooler, more mesic areas and at cold-temperature range boundaries (Beck et al., 2011b; Juday et al., 2015; Ju and Masek, 2016; Pastick et al., 2019), which is consistent with UVAFME predictions of increases in biomass at higher elevations (Fig. 9) and in areas with ample soil moisture and shallow permafrost layers (Fig. A18; A25). Dendrochronological records, however, indicate sensitivity of individuals to increasing evaporative demand (Beck et al., 2011b; Walker and Johnstone, 2014; Juday et al., 2015), especially for those at warmer, dryer sites. UVAFME predictions and remote sensing studies show such areas of vegetation decline as a result of drought and fire mortality (Ju and Masek, 2016; Pastick et al., 2019) (Fig. 9; A11–A14; A21; A22). A dendrochronology study by Sullivan et al. (2017) found that tree response to moisture availability was dependent in part on site conditions such as topography, moss cover, and organic layer depth. UVAFME likewise predicted differing vegetation response to climate change based on elevation and site conditions (Fig. A23-A30). These observation-based studies, along with our results, indicate that forest response to climate change will not be linear or homogenous across interior Alaska, but instead will depend on pre-climate change species composition and site conditions. A fine-scaled model such as UVAFME allows for these impacts to be realized and incorporated into simulations across a large domain.

The UVAFME-predicted shifts towards higher deciduous fraction (Figs. 8,10) could have implications for climate feedbacks. Deciduous forests have a higher albedo than do spruce forests (Beck et al., 2011b), and thus a shift towards higher deciduous fraction could have a net cooling effect on the landscape (Liu et al., 2006; Rogers et al., 2013, 2015). It is also likely that deciduous forests will store less carbon in the soil due to rapid decomposition and nutrient turnover (Johnstone et al., 2010a; Alexander and Mack, 2015) (Fig. A19), thus further interacting with permafrost, vegetation, and wildfire dynamics. Additionally, because deciduous trees and litter are also less flammable than is black spruce litter (Johnson, 1992; Hely et al., 2009), this vegetation shift could also modify the fire regime, resulting in fewer, less severe fires. However, UVAFME also predicted soil drying throughout the region, especially under the RCP 8.5 scenario (Fig. A18), which could lead to increases in fire frequency and intensity. Simulations with ALFRESCO investigating this deciduous fraction-fire severity feedback did find a negative feedback between deciduous cover and fire severity, though this effect was not strong enough to overcome the climate-induced increase in fire frequency when also considering climate warming (Johnstone et al., 2011). Future work with UVAFME will relate fire ignition and spread directly to litter and fire weather conditions, allowing for further interactions between vegetation, soils, fire, and climate.

The simulations presented here did not include the potential CO_2 fertilization effect on tree growth. It is possible that some amount of drought stress caused by increasing evaporative demand may be alleviated by increased water use efficiency provided by elevated CO_2 levels (Sullivan et al., 2017). However, it is unclear how this mechanism may actually occur in trees, and it has been shown that existing models which do incorporate a CO_2 fertilization effect overestimate biomass (Albani et al., 2006), stemming from a lack of simulation of acclimation to elevated CO_2 levels. Thus, without a full understanding of how rising CO_2 levels will impact individual tree growth, we chose to leave out this potential vegetation driver. Future work with UVAFME will test methods for incorporating CO_2 fertilization into the model and will investigate how this additional factor may interact with other drivers of forest change.

In these simulations with UVAFME, insect infestation and forest pathogens were also not included. Studies have shown links between declining quaking aspen growth, moisture deficit, and insect defoliation (Michaelian et al., 2011; Trugman et al., 2017; Cahoon et al., 2018; Boyd et al., 2019). Additionally, data on quaking aspen fungal canker infection show that much of the documented quaking aspen mortality can also be attributed to this pathogen (R. Ruess, *pers. comm.*). An ongoing outbreak of the spruce beetle (*Dendroctonus rufipennis* (Kirby)) in southcentral Alaska has caused widespread spruce mortality and carbon losses (USFS, 2016). The spruce beetle infestations are occurring at a rapidly increasing and northward-expanding rate, and could potentially move north into interior Alaska. Thus, simulations with UVAFME presented here must be considered with these important mortality agents in mind. UVAFME has an existing bark beetle submodel that was applied in the spruce forests of the US Rocky Mountains (Foster et al., 2018), with results showing strong combined effects of climate and insect infestation. Future work with the model in Alaska will include the effects of the spruce beetle as well as other important insects and pathogens. One of the main benefits of using a model like UVAFME to study such complex systems is its ability to simulate individual tree and individual stand response to shifting climate and disturbance regimes, as well as the landscape-scale, emergent properties of such responses across large regions (Bugmann et al., 1996; Foster et al., 2015; Shuman et al., 2017; Shugart et al., 2018).

5. Conclusions

Because the high latitudes are experiencing an accelerated rate of

warming relative to the rest of the globe, the boreal zone of Alaska is particularly vulnerable to the interacting effects of fire, climate, soils, and vegetation. These forests contain a heterogenous mix of climates, soil conditions, and fire regimes, resulting in a mosaic of forest types across the region. Alternative stable forest types arise as a result of the legacy effects of these interacting forest drivers, which are reinforced by species-specific tolerances, litter characteristics, and regeneration strategies. Climate change, however, has the capacity to break these legacy effects, resulting in novel site conditions and species compositions. Our results show that these site- and species-specific conditions are important to consider at an individual tree and stand scale in order to accurately predict both current and future forest dynamics and trajectories. We found evidence for declining black and white spruce biomass, and increasing quaking aspen biomass as a result of increasing temperatures throughout interior Alaska. In cool, moist areas, or at high elevation range boundaries, however, we found evidence for increasing spruce biomass. Thus, it is likely that the mosaic of forest types within Alaska will be altered in the future as a result of changing climate and wildfire regimes, and may lead to prolonged biome shifts. As these forests are a major component of the global C budget and provide ecosystem service functions, such changes will have significant ecological and climate feedback implications regionally and even globally.

Conflict of interest statement

The authors declare no conflicts of interest.

Acknowledgements

We acknowledge support of NASA ABoVE grant NNX17AE44G, DoD SERDP grant RC18-1183, and an appointment to the NASA Postdoctoral Fellowship Program at NASA Goddard Space Flight Center, administered by the Universities Space Research Association under contract with NASA. Computing resources supporting this work were provided by the NASA High-End Computing (HEC) Program through the NASA Center for Climate Simulation (NCCS) at Goddard Space Flight Center. We additionally thank J. Yarie at the Bonanza Creek LTER - University of Alaska Fairbanks for the use of available tree core data associated with the CAFI sites as well as two anonymous reviewers who helped improve the manuscript.

Appendix A. Supplementary data

Supplementary material related to this article can be found, in the online version, at doi:https://doi.org/10.1016/j.ecolmodel.2019.108765.

References

Albani, M., Medvigy, D., Hurtt, G.C., Moorcroft, P.R., 2006. The contributions of land-use change, CO2 fertilization, and climate variability to the Eastern US carbon sink. Glob. Chang. Biol. 12, 2370–2390.

Alexander, H.D., Mack, M.C., 2015. A canopy shift in interior alaskan boreal forests: consequences for above- and belowground carbon and nitrogen pools during post-fire succession. Ecosystems 19, 98–114.

Alexander, H.D., Mack, M.C., Goetz, S., Beck, P.S.A., Belshe, E.F., 2012. Implications of increased deciduous cover on stand structure and aboveground carbon pools of Alaskan boreal forests. Ecosphere 3, art45.

Andersen, H.-E., Strunk, J., Temesgen, H., 2011. Using airborne light detection and ranging as a sampling tool for estimating forest biomass resources in the Upper Tanana Valley of Interior Alaska. West. J. Appl. For. 26, 157–164.

Andreu-Hayles, L., D'Arrigo, R., Anchukaitis, K.J., Beck, P.S., Frank, D., Goetz, S., 2011. Varying boreal forest response to Arctic environmental change at the Firth River, Alaska. Environ. Res. Lett. 6, 045503.

Barber, V.A., Juday, G.P., Finney, B.P., 2000. Reduced growth of Alaskan white spruce in the twentieth century from temperature-induced drought stress. Nature 405, 668–673.

Beck, P.S.A., Goetz, S.J., Mack, M.M., Alexander, H., Jin, Y., Randerson, J.T., 2011a. The impacts and implications of an intensifying fire regime on Alaskan boreal forest composition and albedo. Glob. Chang. Biol. 17, 2853–2866.

Beck, P.S.A., Juday, G.P., Alix, C., Barber, V.A., Winslow, S.E., Sousa, E.E., Heiser, P., Herriges, J.D., Goetz, S.J., 2011b. Changes in forest productivity across Alaska consistent with biome shift. Ecol. Lett. 14, 373–379.

Bennett, A., Lindgren, M., Kurkowski, T., 2017. Scenarios Network for Alaska and Arctic Planning: ALFRESCO Model Outputs - Relative Flammability. October 24. http://ckan.snap.uaf.edu/dataset/alfresco-model-outputs-relative-flammability.

Bernier, P.Y., Gauthier, S., Jean, P.-O., Manka, F., Boulanger, Y., Beaudoin, A., Guindon, L., 2016. Mapping local effects of forest properties on fire risk across Canada. Forests 7, 157.

Boby, L.A., Schuur, E.A.G., Mack, M.C., Verbyla, D., Johnstone, J.F., 2010. Quantifying fire severity, carbon, and nitrogen emissions in Alaska's boreal forest. Ecol. Appl. 20, 1633–1647.

Bonan, G.B., 1989. A computer model of the solar radiation, soil moisture, and soil thermal regimes in boreal forests. Ecol. Modell. 45, 275–306.

Bonan, G.B., 1990. Carbon and nitrogen cycling in North American boreal forests I. Litter quality and soil thermal effects in interior Alaska. Biogeochemistry 10, 1–28.

Bonan, G.B., Korzukhin, M.D., 1989. Simulation of moss and tree dynamics in the boreal forests of interior Alaska. Vegetatio 84, 31–44.

Bond-Lamberty, B., Wang, C., Gower, S.T., 2002. Aboveground and belowground biomass and sapwood area allometric equations for siz boreal trees species of northern Manitoba. Can. J. For. Res. 32, 1441–1450.

Botkin, D.B., 1993. Forest Dynamics: An Ecological Model. Oxford University Press, New York, NY.

Botkin, D.B., Janak, J.F., Wallis, J.R., 1972. Some ecological consequences of a computer model of forest growth. J. Ecol. 60, 849.

Boyd, M.A., Berner, L.T., Doak, P., Goetz, S.J., Rogers, B.M., Wagner, D., Walker, X.J., Mack, M.C., 2019. Impacts of climate and insect herbivory on productivity and physiology of trembling aspen (Populus tremuloides) in Alaskan boreal forests. Environ. Res. Lett.

Bradshaw, C.J., Warkentin, I.G., 2015. Global estimates of boreal forest carbon stocks and flux. Glob. Planet. Change 128, 24–30.

Bugmann, H., Fischlin, A., Kienast, F., 1996. Model convergence and state variable update in forest gap models. Ecol. Modell. 89, 197–208.

Burns, R.M., Honkala, B.H., 1990. Silvics of North America: 1. Conifers; 2. Hardwoods. Agricultural Handbook 654, vol. 2. U.S. Department of Agriculture, Forest Service, Washington, DC, pp. 877.

Cahoon, S.M.P., Sullivan, P.F., Brownlee, A.H., Pattison, R.R., Andersen, H.E., Legner, K., Hollingsworth, T.N., 2018. Contrasting drivers and trends of coniferous and deciduous tree growth in interior Alaska. Ecology 99, 1284–1295.

Camill, P., Lynch, J.A., Clark, J.S., Adams, B., Jordan, B., 2001. Changes in biomass, aboveground net primary production, and peat accumulation following permafrost thaw in the boreal peatlands of Manitoba, Canada. Ecosystems 4, 461–478.

Chapin III, F.S., Hollingsworth, T., Murray, D.F., Viereck, L.A., Walker, M.D., 2006a. Floristic diversity and vegetation distribution in the Alaskan boreal Forest. In: Chapin IIIF.S., Oswood, M.W., Van Cleve, K., Viereck, L.A., Verbyla, D.L. (Eds.), Alaska'S Changing Boreal Forest. Oxford University Press, Oxford, pp. 81–99.

Chapin III, F.S., Trainor, S.F., Cochran, P., Huntington, H., Markon, C., McCammon, M., McGuire, A.D., Serreze, M.C., 2014. Ch. 22: Alaska. In: Melillo, J.M., Richmond, T.C., Yohe, G.W. (Eds.), Climate Change Impacts in the United States: The Third National Climate Assessment. US Global Change Research Program, pp. 514–536.

Chapin III, F.S., Viereck, L.A., Adams, P., Van Cleve, K., Fastie, C.L., Ott, R.A., Mann, D., Johnstone, J.F., 2006b. Successional processes in the Alaskan boreal Forest. In: Chapin, F., Oswood, M., Van Cleve, K., Viereck, L., Verbyla, D. (Eds.), Alaska'S Changing Boreal FOrest. Oxford University Press, New York, pp. 100–120.

Euskirchen, E.S., Bennett, A.P., Breen, A.L., Genet, H., Lindgren, M.A., Kurkowski, T.A., McGuire, A.D., Rupp, T.S., 2016. Consequences of changes in vegetation and snow cover for climate feedbacks in Alaska and northwest Canada. Environ. Res. Lett. 11.

Euskirchen, E.S., McGuire, A.D., Chapin III, F.S., Yi, S., Thompson, C.C., 2009. Changes in vegetation in northern Alaska under scenarios of climate change. Ecol. Appl. 19, 1022–1043.

Fahnestock, G.R., Agee, J.K., 1983. Biomass consumption and smoke production by prehistoric and modern forest fires in western Washington. J. For. 81, 653–656.

Fettig, C.J., Reid, M.L., Bentz, B.J., Sevanto, S., Spittlehouse, D.L., Wang, T., 2013. Changing climates, changing forests: a western North American perspective. J. For. 111, 214–228.

Fisher, J.B., Hayes, D.J., Schwalm, C., Huntzinger, D.N., Stofferahn, E., Schaefer, K., Luo, Y., Wullschleger, S.D., Goetz, S., Miller, C.E., Griffith, P., Chadburn, P., Chatterjee, A., Ciais, P., Douglas, T.A., Genet, H., Ito, A., Neigh, C.S.R., Poulter, B., Rogers, B.M., Sonnentag, O., Tian, H., Wang, W., Xue, Y., Yang, Z., Zhang, Z., 2018. Missing pieces to modeling the Arctic-Boreal puzzle. Environ. Res. Lett. 13, 020202.

Fisher, J.B., Sikka, M., Oechel, W.C., Huntzinger, D.N., Melton, J.R., Koven, C.D., Ahlström, A., Arain, M.A., Baker, I., Chen, J.M., Ciais, P., Davidson, C., Dietze, M., El-Masri, B., Hayes, D., Huntingford, C., Jain, A.K., Levy, P.E., Lomas, M.R., Poulter, B., Price, D., Sahoo, A.K., Schaefer, K., Tian, H., Tomelleri, E., Verbeeck, H., Viovy, N., Wania, R., Zeng, N., Miller, C.E., 2014. Carbon cycle uncertainty in the Alaskan Arctic. Biogeosciences 11, 4271–4288.

Flanagan, P.W., Van Cleve, K., 1983. Nutrient cycling in relation to decomposition and organic matter quality in taiga ecosystems. Can. J. For. Res. 13, 795–817.

Foster, A. C., B. M. Rogers, A. Halota, B. Cook, A. H. Armstrong, K. J. Ranson, and S. J. Goetz. in prep. Combining high-resolution LiDAR and forest modeling to improve predictions of forest state across interior Alaska. Environmental Research Letters.

Foster, A.C., Shugart, H.H., Shuman, J.K., 2015. Model-based evidence for cyclic phenomena in a high-elevation, two-species forest. Ecosystems 19, 437–449.

Foster, A.C., Shuman, J.K., Shugart, H.H., Dwire, K.A., Fornwalt, P.J., Sibold, J., Negron, J., 2017. Validation and application of a forest gap model to the southern Rocky Mountains. Ecol. Modell. 351, 109–128.

Foster, A.C., Shuman, J.K., Shugart, H.H., Negron, J., 2018. Modeling the interactive

effects of spruce beetle infestation and climate on subalpine vegetation. Ecosphere 9, e02437.
Genet, H., McGuire, A.D., Barrett, K., Breen, A., Euskirchen, E.S., Johnstone, J.F., Kasischke, E.S., Melvin, A.M., Bennett, A., Mack, M.C., 2013. Modeling the effects of fire severity and climate warming on active layer thickness and soil carbon storage of black spruce forests across the landscape in interior Alaska. Environ. Res. Lett. 8.
Grosse, G., Harden, J., Turetsky, M., McGuire, A.D., Camill, P., Tarnocai, C., Frolking, S., Schuur, E.A.G., Jorgensen, T., Marchenko, S., Romanovsky, V., Wickland, K.P., French, N., Waldrop, M., Bourgeau-Chavez, L.L., Striegl, R.G., 2011. Vulnerability of high-latitude soil organic carbon in North America to disturbance. Geophys. Res. Lett. 116, G00K06.
Hargreaves, G.H., Samni, Z.A., 1982. Estimation of potential evapotranspiration. J. Irrig. Drain. Div. Proc. Am. Soc. Civil Eng. 108, 223–230.
Harris, I., Jones, P.D., Osborn, T.J., Lister, D.H., 2014. Updated high-resolution grids of monthly climatic observations — the CRU TS3.10 Dataset. Int. J. Climatol. 34, 624–642.
Hely, C., Bergeron, Y., Flannigan, M.D., 2009. Effects of stand composition on fire hazard in mixed-wood Canadian boreal forest. J. Veg. Sci. 11, 813–824.
Hogg, E.H., Brandt, J.P., Michallian, M., 2008. Impacts of a regional drought on the productivity, dieback, and biomass of western Canadian aspen forests. Can. J. For. Res. 38, 610–622.
Holden, S.R., Rogers, B.M., Treseder, K.K., Randerson, J.T., 2016. Fire severity influences the response to soil microbes to a boreal forest fire. Environ. Res. Lett. 11, 035004. https://doi.org/10.1088/1748-9326/11/3/035004.
Hurtt, G.C., Thomas, R.Q., Fisk, J.P., Dubayah, R.O., Sheldon, S.L., 2016. The impact of fine-scale disturbances on the predictability of vegetation dynamics and carbon flux. PLoS One 11, e0152883.
Jensen, M.E., Haise, H.R., 1963. Estimating evapotranspiration from solar radiation. J. Irrig. Drain. Eng. 89, 15–41.
Johnson, E.A., 1992. Fire and Vegetation Dynamics: Studies From the North American Boreal Forest. Cambridge University Press, Cambridge.
Johnstone, J.F., Chapin III, F.S., Hollingsworth, T.N., Mack, M.C., Romanovsky, V., Turetsky, M., 2010a. Fire, climate change, and forest resilience in interior Alaska. Can. J. For. Res. 40, 1302–1312.
Johnstone, J.F., Hollingsworth, T.N., Chapin III, F.S., Mack, M.C., 2010b. Changes in fire regime break the legacy lock on successional trajectories in Alaskan boreal forest. Glob. Chang. Biol. 16, 1281–1295.
Johnstone, J.F., Kasischke, E.S., 2005. Stand-level effects of soil burn severity on postfire regeneration in a recently burned black spruce forest. Can. J. For. Res. 35, 2151–2163.
Johnstone, J.F., Rupp, T.S., Olson, M., Verbyla, D., 2011. Modeling impacts of fire severity on successional trajectories and future fire behavior in Alaskan boreal forests. Landsc. Ecol. 26, 487–500.
Jolly, W.M., Cochrane, M.A., Freeborn, P.H., Holden, Z.A., Brown, T.J., Williamson, G.J., Bowman, D.M.J.S., 2015. Climate-induced variations in global wildfire danger from 1979 to 2013. Nat. Commun. 6, 7537.
Ju, J., Masek, J.G., 2016. The vegetation greenness trend in Canada and US Alaska from 1984-2012 Landsat dat. Remote Sens. Environ. 176, 1–16.
Juday, G.P., Alix, C., Grant III, T.A., 2015. Spatial coherence and change of opposite white spruce temperature sensitivities on floodplains in Alaska confirms early-stage boreal biome shift. For. Ecol. Manage. 350, 46–61.
Jumikis, A.R., 1966. Thermal Soil Mechanics. Rutgers University Press, New Burnswick, NJ.
Kasischke, E.S., O'Neill, K.P., French, N.H.F., Bourgeau-Chavez, L.L., 2000. Controls on patterns of biomass burning in Alaskan boreal forests. In: Kasischke, E.S., Stocks, B.J. (Eds.), Fire, Climate Change, and Carbon Cycling in the Boreal Forest. Springer-Verlag, New York, NY, pp. 173–196.
Kasischke, E.S., Williams, D., Barry, D., 2002. Analysis of the patterns of large fires in the boreal forest region of Alaska. Int. J. Wildland Fire 11, 131–144.
Kasischke, E.S., Verbyla, D.L., Rupp, T.A., McGuire, A.D., Murphy, K.A., Jandt, R., Barnes, J.L., Hoy, E.E., Duffy, P.A., Calef, M., Turetsky, M., 2010. Alaska's changing fire regime - implications for vulnerability of its boreal forests. Can. J. For. Res. 40, 1313–1324.
Keane, R.E., Austin, M., Field, C., Huth, A., Lexer, M.J., Peters, D., Solomon, A., Wyckoff, P., 2001. Tree mortality in gap models: application to climate change. Clim. Change 51, 509–540.
Keane, R.E., Loehman, R.A., Holsinger, L.M., 2011. The FireBGCv2 Landscape Fire Succession Model: a research simulation platform for exploring fire and vegetation dynamics. USDA For. Serv. Gen. Tech. Rep. RMRS-GTR-55 145.
Lambert, A., Ung, C., Raulier, F., 2005. Canadian national tree aboveground biomass equations. Can. J. For. Res. 35, 1996–2018.
Leonawicz, M., Lindgren, M., Kurkowski, T., Walsh, J., Rupp, S., 2015a. Projected Monthly and Derived Temperature Products - 771 M CMIP5/AR5. Scenarios Network for Alaska and Arctic Planning (SNAP).
Leonawicz, M., Lindgren, M., Kurkowski, T., Walsh, J., Rupp, S., 2015b. Projected Monthly and Derived Precipitation Products - 771 M CMIP5/AR5. Scenarios Network for Alaska and Arctic Planning (SNAP).
Lindgren, M., Kurkowski, T., 2012. Scenarios Network for Alaska and Arctic Planning (SNAP) : Elevation. November 6. http://data.snap.uaf.edu/data/IEM/Inputs/ancillary/elevation/.
Liu, B.Y.H., Jordan, R.C., 1962. Daily insoluation on surfaces tilted towards the equator. Am. Soc. Heat. Refrig. Air-Condition. Eng. 67, 526–541.
Liu, Z., Notaro, M., Kutzbach, J., Liu, N., 2006. Assessing global vegetation-climate feedbacks from observations. J. Clim. 19, 787–814.
Lunardini, V.J., 1981. Heat Transfer in Cold Climates. Van Nostrand Reinhold, New York.
Fauria, Macias, Johnson, E.A., 2006. Large-scale climatic patterns control large lightning fire occurrence in Canada and Alaska forest regions. J. Geophys. Res. 111.
Malone, T., Liang, J., Packee, E.C., et al., 2009. Cooperative Alaska Forest Inventory. US Department of Agriculture, Forest Service, Pacific Northwest Research Station.
Mekonnen, Z.A., Riley, W., Randerson, J., Grant, R.F., Rogers, B.M., 2019. Expansion of high-latitude deciduous forests driven by interactions between climate warming and fire. Nat. Plants.
Melillo, J.M., Richmond, T.C., Yohe, G.W. (Eds.), 2014. Climate Change Impacts in the United States: The Third National Climate Assessment. US Global Change Research PRogram, Washington, D.C.
Michaelian, M., Hogg, E.H., Hall, R.J., Arsenault, E., 2011. Massive mortality of aspen following severe drought along the southern edge of the Canadian boreal forest. Glob. Chang. Biol. 17, 2084–2094.
Nikolov, N., Helmisaari, H., 1992. Silvics of the circumpolar boreal forest tree species. In: Shugart, H.H., Leemans, R., Bonan, G.B. (Eds.), A Systems Analysis of the Global Boreal Forest. Cambridge University Press, Cambridge, UK, pp. 13–84.
Olnes, J., Kielland, K., 2016. Stage-dependent effects of browsing by snowshoe hares on successional dynamics in a boreal forest ecosystem. Ecosphere 7, e01475.
Overland, J.E., Hanna, E., Hanssen-Bauer, I., Kim, S.-J., Walsh, J.E., Wang, M., Bhatt, U.S., Thoman, R.L., 2016. Surface Air Temperature. NOAA.
Pastick, N.J., Duffy, P., Genet, H., Rupp, T.S., Wylie, B.K., Johnson, K.D., Jorgenson, M.T., Bliss, N., McGuire, A.D., Jafarov, E.E., Knight, J.F., 2017. Historical and projected trends in landscape drivers affecting carbon dynamics in Alaska. Ecol. Appl. 27, 1–20.
Pastick, N.J., Jorgensen, M.T., Goetz, S.J., Jones, B.M., Wylie, B.K., Minsley, B.J., Genet, H., Knight, J.F., Swanson, D.K., Jorgenson, J.C., 2019. Spatiotemporal remote sensing of ecosystem change and causation across Alaska. Glob. Chang. Biol. 25, 1171–1189.
Pastor, J., Post, W.M., 1985. Development of a Linked Forest Productivity-soil Process Model. Page 108. Environmental Sciences Division Publication, USDA, Oak Ridge National Laboratory.
Payette, S., 1992. Fire as a controlling process in the North American boreal forest. In: Shugart, H.H., Leemans, R., Bonan, G.B. (Eds.), A Systems Analysis of the Global Boreal Forest. Cambridge University Press, Cambridge, UK, pp. 144–169.
Purves, D., Pacala, S., 2008. Predictive models of forest dynamics. Science 320, 1452–1453.
Rogers, B.M., Randerson, J.T., Bonan, G.B., 2013. High-latitude cooling associated with landscape changes from North American boreal forest fires. Biogeosciences 10, 699–718.
Rogers, B.M., Soja, A.J., Goulden, M.L., Randerson, J.T., 2015. Influence of tree species on continental differences in boreal fires and climate feedbacks. Nat. Geosci. 8, 228–234.
Rogers, B.M., Solvik, K., Hogg, E.H., Ju, J., Masek, J.G., Michaelian, M., Berner, L.T., Goetz, S.J., 2018. Detecting early warning signals of tree mortality in boreal North America using multiscale satellite data. Glob. Chang. Biol. 24, 2284–2304.
Rogers, B.M., Veraverbeke, S., Azzari, G., Czimczik, C.I., Holden, S.R., Mouteva, G.O., Sedano, F., Treseder, K.K., Randerson, J.T., 2014. Quantifying fire-wide carbon emissions in interior Alaska using field measurements and Landsat imagery. J. Geophys. Res. Biogeosci. 119, 1608–1629.
Rosenberg, N.J., Blad, B.L., Verma, S.B., 1983. Microclimate. Wiley, New York.
Rothermel, R.C., 1972. A Mathematical Model for Predicting Fire Spread in Wildland Fuels. Page 50. Reasearch Paper INT, USDA Forest Service Intermountain Forest and Range Experiment Station, Ogden, UT.
Ruess, R.W., 2015. Organic Horizon Depth in the Regional Site Network 606 Bonanza Creek LTER - University of Alaska Fairbanks: BNZ.
Rupp, T.S., Chen, X., Olson, M., 2007. Sensitivity of simulated boreal fire dynamics to uncertainties in climate drivers. Earth Interact. 11, 1–21.
Schumacher, S., Reineking, B., Sibold, J., Bugmann, H., 2006. Modeling the impact of climate and vegetation on fire regines in mountain landscapes. Landsc. Ecol. 21, 539–554.
Shugart, H.H., 1984. A Theory of Forest Dynamics: The Ecological Implications of Forest Succession Models. Springer Science & Business Media, New York, NY.
Shugart, H.H., Leemans, R., Bonan, G.B., 1992. A Systems Analysis of the Global Boreal Forest. Cambridge University Press, Cambridge, UK.
Shugart, H.H., Seagle, S.W., 1985. Modeling forest landscapes and the role of disturbance in ecosystems and communities. In: Pickett, S.T.A., White, P.S. (Eds.), The Ecology of Natural Disturbance and Patch Dynamics. Elsevier, pp. 353–368.
Shugart, H.H., Wang, B., Fischer, R., Ma, J., Fang, J., Yan, X., Huth, A., Armstrong, A., 2018. Gap models and their individual-based relativesin the assessment of the consequences of global change. Environ. Res. Lett. 13.
Shugart, H.H., Woodward, F.I., 2011. Global Change and the Terrestrial Biosphere. Wiley-Blackwell, Sussex, UK.
Shuman, J.K., Foster, A.C., Shugart, H.H., Hoffman-Hall, A., Krylov, A., Loboda, T., Ershov, D., Sochilova, E., 2017. Fire disturbance and climate change: implications for Russian forests. Environ. Res. Lett. 12.
Shuman, J.K., Shugart, H.H., Krankina, O.N., 2014. Testing individual-based models of forest dynamics: issues and an example from the boreal forests of Russia. Ecol. Modell. 293, 102–110.
Shuman, J.K., Tchebakova, N., Parfenova, E., Soja, A., Shugart, H.H., Ershov, E., Holcomb, H., 2015. Forest forecasting with vegetation models across Russia. Can. J. For. Res. 45, 175–184.
Sullivan, P.F., Pattison, R.R., Brownlee, A.H., Cahoon, S.M.P., Hollingsworth, T.N., 2017. Limited evidence of declining growth among moisture-limited black and white spruce in interior Alska. Sci. Rep. 7.
Thonicke, K., Spessa, A., Harrison, S.P., Dong, L., Carmona-Moreno, C., 2010. The influence of vegetation, fire spread and fire behaviour on biomass burning and trace gas emissions: results from a process-based model. Biogeosciences 7, 1991–2011.
Trugman, A.T., Medvigy, D., Anderegg, W.R.L., Pacala, S.W., 2017. Differential declines in Alaskan boreal forest vitality related to climate and competition. Glob. Chang. Biol.

Ung, C.-H., Bernier, P., Guo, X.-J., 2008. Canadian national biomass equations: new parameter estimates that include British Columbia data. Can. J. For. Res. 38, 1123–1132.
USFS, 2016. Forest Health Conditions in Alaska - 2016: a Forest Health Protection Report. Page 76. USDA Forest Service State of Alaska Department of Natural Resources Division of Forestry, Anchorage, AK.
Van Cleve, K., Viereck, L.A., 1981. Forest succession in relation to nutrient cycling in the boreal forest of Alaska. In: West, D.C., Shugart, H.H., Botkin, D.B. (Eds.), Forest Succession. Concepts and Applications. Springer-Verlag, New York, NY, pp. 185–211.
Vance, E.D., Chapin III, F.S., 2001. Substrate limitations to microbial activity in taiga forest floors. Soil Biol. Biochem. 33, 173–188.
Viereck, L.A., Dyrness, C.T., Van Cleve, K., Foote, M.J., 1983. Vegetation, soils, and forest productivity in selected forest types in interior Alaska. Can. J. For. Res. 13, 703–720.
Viereck, L.A., Little, E.L., 2007. Alaska Trees and Shrubs, second edition. University of Alaska Press, Fairbanks, AK.
Viereck, L.A., Van Cleve, K., Dyrness, C.T., 1986. Forest ecosystem distribution in the taiga environment. In: Van Cleve, K., Chapin IIIF.S.I., Flanagan, P.W., Viereck, L.A., Dyrness, C.T. (Eds.), Forest Ecosystems in the Alaskan Taiga. Springer, New York, pp. 22–43.
Vogel, J.G., 2007. Black Spruce C Cycling Study Along a Temperature Gradient in Interior Alaska. Bonanza Creek LTER - University of Alaska Fairbanks, BNZ, pp. 304.
Walker, X., Johnstone, J.F., 2014. Widespread negative correlations between black spruce growth and temperature across topographic moisture gradients in the boreal forest. Environ. Res. Lett. 9, 064016.
Wang, B., Shugart, H.H., Lerdau, M.T., 2017. An individual-based model of forest volatile organic compound emissions-UVAFME-VOC v1.0. Ecol. Modell. 350, 69–78.
Wang, T.A., Hamann, A., Spittlehouse, D., Carroll, C., 2016. Locally downscaled and spatially customizable climate data for historical and future periods for North America. PLoS One 11.
Wasser, L., Day, R., Chasmer, L., Taylor, A., 2013. Influence of vegetation structure on lidar-derived canopy height and fractional cover in forested riparian buffers during leaf-of and leaf-on. PLoS One 8.
Yan, X., Shugart, H.H., 2005. FAREAST: a forest gap model to simulate dynamics and patterns of eastern Eurasian forests: simulation of eastern Eurasian forests. J. Biogeogr. 32, 1641–1658.
Yarie, J., 1998. Soil Physical and Chemical Properties Based on Genetic Horizon From 4 Replicate Pits Placed Around Replicate LTER Control Plots Sampled in 1988 and 1989. Bonanza Creek LTER - University of Alaska Fairbanks, BNZ, pp. 134.
Yarie, J., Kane, E., Mack, M.C., 2007. Aboveground Biomass Equations for Trees of Interior Alaska. USFS Agricultural and Forestry Experiment Station Bulletin, University of Alaska, Fairbanks, AK.
Yarie, J., Viereck, L., Van Cleve, K., Adams, P., 1998. Flooding and ecosystem dynamics along the Tanana River. BioScience 48, 690–695.
Zasada, J.C., Sharik, T.L., Nygren, M., 1992. The reproductive process in boreal forest trees. In: Shugart, H.H., Leemans, R., Bonan, G.B. (Eds.), A Systems Analysis of the Global Boreal Forest. Cambridge University Press, Cambridge, UK, pp. 85–125.
Zhu, Z., McGuire, A.D., 2016. Baseline and Projected Future Carbon Storage and Greenhouse-Gas Fluxes in Ecosystems of Alaska. Page 208. Professional Paper, US Geological Survey, Reston, VA.